

1 Time dependent source apportionment of submicron organic  
2 aerosol for a rural site in an alpine valley using a rolling PMF  
3 window

4 Gang Chen<sup>1</sup>, Yulia Sosedova<sup>1,2</sup>, Francesco Canonaco<sup>1,2</sup>, Roman Fröhlich<sup>1</sup>, Anna Tobler<sup>1,2</sup>,  
5 Athanasia Vlachou<sup>1</sup>, Kaspar R. Daellenbach<sup>1</sup>, Carlo Bozzetti<sup>2</sup>, Christoph Hueglin<sup>3</sup>, Peter Graf<sup>3</sup>,  
6 Urs Baltensperger<sup>1</sup>, Jay G. Slowik<sup>1</sup>, Imad El Haddad<sup>1</sup>, and André S.H. Prévôt<sup>1\*</sup>

7 <sup>1</sup>Laboratory of Atmospheric Chemistry, Paul Scherrer Institute, CH-5232 Villigen PSI,  
8 Switzerland

9 <sup>2</sup>Datalystica Ltd., Park innovAARE, CH-5234 Villigen, Switzerland

10 <sup>3</sup>Empa, Swiss Federal Laboratories for Materials Science and Technology, Laboratory for Air  
11 Pollution and Environmental Technology, CH-8600 Dübendorf, Switzerland

12 \*Correspondence to: André S. H. Prévôt (andre.prevot@psi.ch)

13

## Abstract

We collected one year of aerosol chemical speciation monitor (ACSM) data in Magadino, a village located in the south of the Swiss Alpine region, one of Switzerland's most polluted areas. We analysed the mass spectra of organic aerosol (OA) by positive matrix factorisation (PMF) using source finder professional (SoFi Pro) to retrieve the origins of OA. Therein, we deployed the rolling algorithm to account for the temporal changes of the source profiles, which is closer to the measurement. As the first-ever application of rolling PMF with ME-2 analysis on a yearlong dataset that was collected from a rural site, we resolved two primary OA factors (traffic-related hydrocarbon-like OA (HOA) and biomass burning OA (BBOA)), one mass-to-charge ratio ( $m/z$ ) 58 related OA (58-OA) factor, a less oxidised oxygenated OA (LO-OOA) factor, and a more oxidised oxygenated OA (MO-OOA) factor. HOA showed stable contributions to the total OA through the whole year ranging from 8.1 to 10.1%, while the contribution of BBOA showed an apparent seasonal variation with a range of 8.3–27.4% (highest during winter, lowest during summer) and a yearly average of 17.1%. OOA (sum of LO-OOA and MO-OOA) contributed 71.6% of the OA mass, varying from 62.5% (in winter) to 78% (in spring and summer). The 58-OA factor mainly contained nitrogen related variables which only appeared to be pronounced after filament switched. However, since the contribution of this factor was insignificant (2.1%), we did not attempt to interpolate its potential source in this work. The uncertainties ( $\sigma$ ) for the modelled OA factors (i.e., rotational uncertainty and statistical variability of the sources) varied from  $\pm 4\%$  (58-OA) to a maximum of  $\pm 40\%$  (LO-OOA). Considering that BBOA and LO-OOA (showing influences of biomass burning in winter) had significant contributions to the total OA mass, we suggest reducing and controlling the residential heating as a mitigation strategy for better air quality and lower PM levels in this region or similar locations. In Appendix A, we conducted a head-to-head comparison between the conventional seasonal PMF analysis and the rolling mechanism. We found similar or

slightly improved results in terms of mass concentrations, correlations with external tracers and factor profiles of the constrained POA factors. The rolling results show smaller scaled residuals and enhanced correlations between OOA factors and corresponding inorganic salts than those of the seasonal solutions, which was most likely because the rolling PMF analysis can capture the temporal variations of the oxidation processes for OOA components. Specifically, the time dependent factor profiles of MO-OOA and LO-OOA can well explain the temporal variabilities of two main ions for OOA factors,  $m/z$  44 ( $\text{CO}_2^+$ ) and  $m/z$  43 (mostly  $\text{C}_2\text{H}_3\text{O}^+$ ). Therefore, this rolling PMF analysis provides a more realistic source apportionment (SA) solution with time dependent OA sources. The rolling results also show good agreement with offline Aerodyne aerosol mass spectrometer (AMS) SA results from filter samples, except for winter. The latter discrepancy is likely because the online measurement can capture the fast oxidation processes of biomass burning sources, in contrast to the 24-hour filter samples. This study demonstrates the strengths of the rolling mechanism and provides a comprehensive criterion list for ACSM users to obtain reproducible SA results, and is a role model for similar analyses of such worldwide available data.

## **1 Introduction**

Atmospheric particulate matter (PM) affects human health and climate. In particular, it influences the radiative balance (IPCC, 2014; von Schneidmesser et al., 2015), reduces visibility (Chow et al., 2002; Horvath, 1993), and negatively affects human health by triggering respiratory and cardiovascular diseases and allergies (Daellenbach et al., 2020; Dockery and Pope, 1994; Mauderly and Chow, 2008; Monn, 2001; Pope and Dockery, 2006; von Schneidmesser et al., 2015). Fine PM exposure strongly correlates with the global mortality rate. Lelieveld et al. (2015) estimated that outdoor air pollution, mostly  $\text{PM}_{2.5}$  (PM with an aerodynamic diameter smaller than  $2.5\ \mu\text{m}$ ), causes 3.3 million premature deaths per year

worldwide. Despite this correlation, different aerosol sources may have strongly different effects on health (Daellenbach et al., 2020). Thus, both climate and health effects are affected by particle chemical composition, which is related to emission sources of primary particles and precursor gases for secondary aerosol (IPCC, 2014; Jacobson et al., 2000; Jacobson, 2001; Lelieveld et al., 2015; Ramanathan et al., 2005).

Organic aerosol (OA) constitutes 20–90% of fine PM (Jimenez et al., 2009; Murphy et al., 2006; Zhang et al., 2007) and contains millions of chemical compounds. Since OA is subject of an extremely complex mixture of chemical constituents, with highly dynamic spatial and temporal (seasonal, diurnal, etc.) variability of directly emitted particles and gas-phase precursors and a complex chemical processing in the atmosphere, elucidation of the chemical composition and physical properties of OA remains challenging. Identification and quantification of OA sources with a sophisticated interpolation of spatial and temporal variabilities are essential for developing effective mitigation strategies for air pollution and a better assessment of the aerosol effect on both health and climate.

OA source apportionment (SA) and PM composition have been studied extensively using the Aerodyne aerosol mass spectrometer (AMS) (Canagaratna et al., 2007). However, due to the complexity of the AMS measurements and their high operational expenses, AMS campaigns are often limited to short periods of a few weeks to months. The aerosol chemical speciation monitor (ACSM) allows for unattended long-term observation (>1 year) of non-refractory aerosol particles (Ng et al., 2011a; Fröhlich et al., 2013). It also makes it possible to investigate the long-term temporal variations of OA sources, which is crucial for policymakers to introduce or validate aerosol-related environmental policies.

Positive matrix factorisation (PMF, see Section 3.1 in the Supplement) has been used in various studies for SA of OA (Lanz et al., 2007; Aiken et al., 2009; Hildebrandt et al., 2011; Zhang et

al., 2011; Mohr et al., 2012; Schurman et al., 2015). The multilinear engine (ME-2) implementation of PMF (Paatero, 1999) improves model performance by allowing the use of *a priori* information (constraints on source profiles and/or time series) to direct the model towards environmentally meaningful solutions (Canonaco et al., 2013; Crippa et al., 2014; Fröhlich et al., 2015; Lanz et al., 2008; Ripoll et al., 2015). For long-term data (one year or more) with high time resolution, the composition of a given source could change considerably due to the meteorological and seasonal variabilities. However, a major limitation of PMF is the assumption of static factor profiles, such that it fails to respond to these temporal changes. Therefore, long-term chemically speciated data have been evaluated monthly or seasonally (Petit et al., 2014; Canonaco et al., 2015; Minguillón et al., 2015; Ripoll et al., 2015; Bressi et al., 2016; Reyes-Villegas et al., 2016) to at least take the seasonal variations into account. To improve the analysis of long-term ACSM datasets, a novel approach that utilises PMF analysis on a shorter time rolling window was first proposed by Parworth et al. (2015) and further refined using ME-2 by Canonaco et al. (2021). The short length of the rolling PMF window allows the PMF model to take the temporal variations of the source profiles into account (e.g., biogenic versus domestic burning influences on oxygenated organic aerosol (OOA)), which normally provides better separation between OA factors. In addition, using this technique together with bootstrap resampling and a random *a*-value approach allows users to assess the statistical and rotational uncertainties of the PMF results (Canonaco et al., 2021; Tobler et al., 2020).

In this work, we conducted a one-year ACSM measurement from September 2013 to October 2014 in Magadino, located in an alpine valley in southern Switzerland. We present a comprehensive analysis of the ACSM dataset measured in Magadino using a novel PMF technique, the “rolling PMF”. In addition, we also compare the results of the rolling PMF with

the source apportionment of offline AMS filter samples (Vlachou et al., 2018) and conventional seasonal PMF analysis.

## 2 Methodology

### 2.1 Sampling site

Magadino is in a Swiss alpine valley (46°90'37'' N, 85°60'2'' E, 204 m.a.s.l.), where the sampling site located. This site belongs to the Swiss National Air Pollution Monitoring Network (NABEL, <https://www.empa.ch/web/s503/nabel>). It is around 1.4 km away from the local train station, Cadenazzo, around 7 km away from the Locarno Airport, and nearly 8 km away from Lake Maggiore. This station is surrounded by agricultural fields within a rural area and is considered as a rural background site. It can be potentially affected by domestic wood burning, adjacent agricultural activity and transit traffic through the valley. The site topography favours quite high PM levels due to stagnant meteorological conditions or boundary layer inversions, especially in winter. Magadino remains one of the most polluted regions in Switzerland, and it often exceeded the annual average PM<sub>10</sub> limit value for Switzerland (20 µg·m<sup>-3</sup>) (Meteotest, 2017; The Swiss Federal Council, 2018). Therefore, there is an increasing need for a more effective mitigation strategy.

### 2.2 ACSM measurements

This study measured chemical composition and mass loadings of non-refractory constituents of ambient submicron aerosol particles (NR-PM<sub>1</sub>) by an Aerodyne quadrupole ACSM (Ng et al., 2011a). The ACSM uses the same sampling and detection technology as the AMS but is simplified and designated for long-term monitoring applications by reducing maintenance frequency at the cost of lower sensitivity, restriction to integer mass resolution, and no size measurement. Same as for the AMS, sampled submicron particles enter the instrument through a critical orifice (100 µm I.D.) at a flow rate of 1.4 cm<sup>3</sup> s<sup>-1</sup> (at 20 °C and 1 atm). The sampling

flow will pass either through a particle filter or directly into the system using an automated 3-way switching valve that is switched every ~30 s. An aerodynamic lens focuses the sampled particles into a narrow beam which impact on a tungsten surface of around 600 °C, where the non-refractory particles vaporise and are subsequently ionised by an electron impact source (70 eV). A quadrupole mass-spectrometer detects the resulting ions up to a mass-to-charge ratio ( $m/z$ ) of 148 Th. The particle mass spectrum is represented by the difference between the total ambient air and particle-free signals.

The quantification of ACSM data requires an estimation of the fraction of NR-PM<sub>1</sub> that bounces off the oven without being vaporised and therefore is not detected (Canagaratna et al., 2007; Matthew et al., 2008). In this study, a constant collection efficiency (CE) factor of 0.45 was applied to take it into account. The details of determinations of CE value was described in Section 1 in the Supplement. In this study, we recorded the data with a time resolution of 30 minutes. During the campaign, the ACSM filament burnt out on 14 April 2014. This was addressed by switching to the backup filament installed within the instrument (no venting required). Calibration of the relative ionisation efficiencies (RIE) of particulate nitrate, sulphate, and ammonium were conducted using size-selected (300 nm) pure NH<sub>4</sub>NO<sub>3</sub> and pure (NH<sub>4</sub>)<sub>2</sub>SO<sub>4</sub> particles. Calibrations of the RIE,  $m/z$  scale, and the sampling flow were performed every 2 months. In this study, we used the averaged RIEs for nitrate, sulphate, and ammonium. The exact values are shown in **Fig S1** of the Supplement.

## 2.3 Complementary measurements

Meteorological data, including temperature, precipitation, wind speed, wind direction, and solar radiation, are monitored at the NABEL station. In addition, concentrations of trace gases (SO<sub>2</sub>, O<sub>3</sub>, NO<sub>x</sub>), equivalent black carbon (eBC), and PM<sub>10</sub> were measured with a time resolution of 10 minutes. We used an aethalometer (AE 31 model by Magee Scientific Inc.) to measure

eBC concentrations. Therefore, we conducted SA of eBC by following Zotter et al. (2017) using Ångström exponents for eBC from traffic  $\alpha_{tr} = 0.9$  and wood burning  $\alpha_{wb} = 1.68$ . More details about eBC source apportionment are provided in Section 2 of the Supplement.

## 2.4 Preparation of the data and error matrices for PMF

In this study, we used acsm\_local\_1610 software (Aerodyne Research Inc.) to prepare the PMF input matrix. In total, this dataset includes 19'708 time points and 67 ions. Of these,  $\text{CO}_2^+$ -related variables ( $I_{\text{O}^+}$  ( $m/z = 16$ ),  $I_{\text{HO}^+}$  ( $m/z = 17$ ), and  $I_{\text{H}_2\text{O}^+}$  ( $m/z = 18$ )) were excluded from the spectral matrix prior to a PMF analysis. They are reinserted into the OA factor mass spectra after the PMF analysis using the ratio from the fragmentation table (Allan et al., 2004); the factor concentrations are likewise adjusted. According to Allan et al. (2003, 2004), the measurement error matrix was calculated with a minimum error considered for the uncertainty of all variables in the data matrix as in Ulbrich et al. (2009). Following the recommendations in Paatero and Hopke (2003) and Ulbrich et al. (2009), the measurement uncertainty for variables ( $m/z$ ) with a signal-to-noise ratio ( $S/N$ )  $< 2$  (weak variables) and  $S/N < 0.2$  (bad variables) were increased by a factor of 2 and 10, respectively. In total, 27 weak ACSM variables were down-weighted. Additionally,  $m/z$  12 and 13 were not considered during the PMF analyses due to being noisy and their overall negative signal. Moreover,  $m/z$  15 was not only very noisy ( $S/N = 0.09$ ) but maybe also affected by high biases due to potential interference with air signals.

## 2.5 Rolling PMF analysis with ME-2

In this study, we conducted a series of steps (Section 3.2 and 3.3 in the Supplement) to obtain the results we presented in this manuscript. In summary, we first tested potential sources for each season with seasonal PMF *pre-tests*. Secondly, we obtained stable seasonal solutions from bootstrap seasonal analysis. Then, we conducted rolling PMF with certain settings (constraints,



number of repeats, length of the window size, and step of rolling window). Lastly, we were able to retrieve robust results using specific criteria to define environmental reasonable solutions. Please refer to Section 3.2 and 3.3 in the Supplement for more detailed description of each step. This section focuses on the general introduction of rolling PMF with ME-2, the differences between our method vs. the method developed by Canonaco et al. (2021), and the general settings of the rolling PMF analysis in this study.

Running PMF over the long-term ACSM datasets assumes that the OA source profiles are static within this time window. It can lead to large errors since OA chemical fingerprints are expected to vary over time (Paatero et al., 2014). For example, Canonaco et al. (2015) showed that summer and winter OOA variability cannot be accurately represented by a single pair of OOA profiles. A common way to reduce the model uncertainty arising from this source is to choose a proper number of OA factors (Sug Park et al., 2000) and then perform a PMF analysis on a subset of measurements to capture temporal features of OA chemical fingerprints. Such characterisation of OA sources on a seasonal basis has been demonstrated in several studies (Lanz et al., 2008; Crippa et al., 2014; Petit et al., 2014; Minguillón et al., 2015; Ripoll et al., 2015; Zhang et al., 2019). Parworth et al. (2015) introduced the rolling PMF by running PMF on a small window (14 days), which advanced with a step of 1 day. This novel technique enables the source profiles to adapt to the temporal variabilities. Canonaco et al. (2021) combined the rolling PMF technique with ME-2 (Section 3.1 in the Supplement) to deal with the rotational ambiguity of the PMF analysis. In addition, it also used the bootstrap resampling strategy (Efron, 1979) and random  $a$ -values (Section 3.2.2 in the Supplement) to estimate the statistical and rotational uncertainties of the PMF analysis.

This study mostly followed the methods developed by Canonaco et al. (2021), but with some modifications. The settings of the rolling PMF window is explicitly explained in Section 3.2.3 of the Supplement). In addition, we also performed a test of rolling window size (i.e., 1, 7, 14,

and 28 days) using a similar approach (Section 4 in the Supplement). As Canonaco et al. (2021) did, we also used the criteria-based selection function developed by Canonaco et al. (2021) to evaluate our PMF runs. The settings of the criteria are provided in Section 3.2.4 of the Supplement.

However, instead of using published reference factor profiles like Canonaco et al. (2021) have done, we retrieved the reference profiles of primary and local factors from seasonal bootstrap analysis (Section 3.2 in the Supplement). Specifically, the reference profiles of hydrocarbon-like OA (HOA) factor and biomass burning OA (BBOA) factor were retrieved from winter (December, January, and February, DJF) bootstrapped PMF solution as shown in **Fig. S4**, and we got the  $m/z$  58 related (58-OA) factor profile from summer (June, July, and August, JJA) bootstrapped PMF solution (**Fig. S4**). The 58-OA was dominated by nitrogen-containing fragments (at  $m/z$  58, 84, and 98). In general, ACSM estimates organic  $m/z$  98 signal by dividing organic  $m/z$  84 to a factor of 2 according to the fragmentation table of organic species that was provided by Allan et al. (2004). Thus, the intensity of  $m/z$  98 is always half of the intensity of  $m/z$  84 in each factor. This 58-OA only appeared after the filament was switched on 14 April 2014. The instrument setup thus strongly influenced the sensitivity of these components due to influences of surface ionisation. The nitrogen-containing ion,  $m/z$  58, was also observed in Hildebrandt et al. (2011) due to the enhanced surface ionisation in a certain period. In addition, the potassium signal enhanced at the same time, which further corroborated our hypothesis of the enhanced surface ionisation. Also, since this factor was constrained through the whole dataset, the PMF model overestimated the mass concentration of this factor significantly, which leads to high uncertainties for the 58-OA. Therefore, the time series of this source should be considered as the upper limit, and the real mass concentration of it could be substantially lower. However, with the low mass concentration of the 58-OA during the whole campaign, we considered it as a minor factor. Thus, this factor was considered in the PMF

analysis, but no further interpretation of its potential source will be attempted in this manuscript. Moreover, we took a different path to define “good” PMF solutions by using a novel student *t*-test approach to determine the environmentally reasonable solutions quantitatively with minimum subjective judgements (Section 3.3 in the Supplement). Overall, we provided a comprehensive analysis of a long-term ACSM dataset using this state-of-the-art technique in this work. The results were unfolded in the following section.

### 3 Results and discussion

#### 3.1 Overview of PM<sub>1</sub> sources in Magadino

Considering that the major part of eBC is within PM<sub>1</sub> (Schwarz et al., 2013), we added eBC to the total NR-PM<sub>1</sub> from the ACSM to perform a mass closure analysis using independent measurements of PM<sub>2.5</sub>/PM<sub>10</sub> from filters. The gravimetric PM<sub>2.5</sub> and PM<sub>10</sub> show a high correlation with the total estimated PM<sub>1</sub> (NR-PM<sub>1</sub> + eBC) (**Fig. S1c**). The slopes of the linear fits ( $\pm 1$  standard deviation) are  $1.62 \pm 0.05$  ( $R^2 = 0.81$ ,  $N=79$ ) for PM<sub>2.5</sub> vs. PM<sub>1</sub> and  $1.84 \pm 0.03$  ( $R^2 = 0.67$ ,  $N=335$ ) for PM<sub>10</sub> vs. PM<sub>1</sub>. It means that the estimated PM<sub>1</sub> comprised 62% and 54% of the PM<sub>2.5</sub> and PM<sub>10</sub> mass, respectively. The daily averages of inorganic species concentrations measured by the ACSM and those measured on the filters by ion chromatography showed a good correlation, with  $R^2 = 0.83$  for SO<sub>4</sub><sup>2-</sup>,  $R^2 = 0.82$  for NO<sub>3</sub><sup>-</sup> and  $R^2 = 0.50$  for Cl<sup>-</sup>, with slopes close to 1 (**Fig. S1a**). The 2-week average of total ammonium and total nitrate measured by the offline AMS technique agreed rather well with the ACSM ammonium ( $R^2 = 0.47$ ) and nitrate ( $R^2 = 0.79$ ), as shown in the plots in **Fig. S1b**. The ion balance of particulate ammonium, sulphate and nitrate measured by the ACSM showed that the measured aerosol particles were mostly neutral.

The daily average PM<sub>1</sub> components are shown in **Fig. 1a**, with an annual average PM<sub>1</sub> concentration (including eBC) from September 2013 to October 2014 equal to 10.2  $\mu\text{g m}^{-3}$ . In

winter, the average PM<sub>1</sub> concentration was highest (13.8 µg·m<sup>-3</sup>), with OA contributing 54% to the total PM<sub>1</sub> mass. In summer, the average PM<sub>1</sub> mass concentration was below 10 µg·m<sup>-3</sup>, but the relative contribution of the OA fraction increased to 62%.

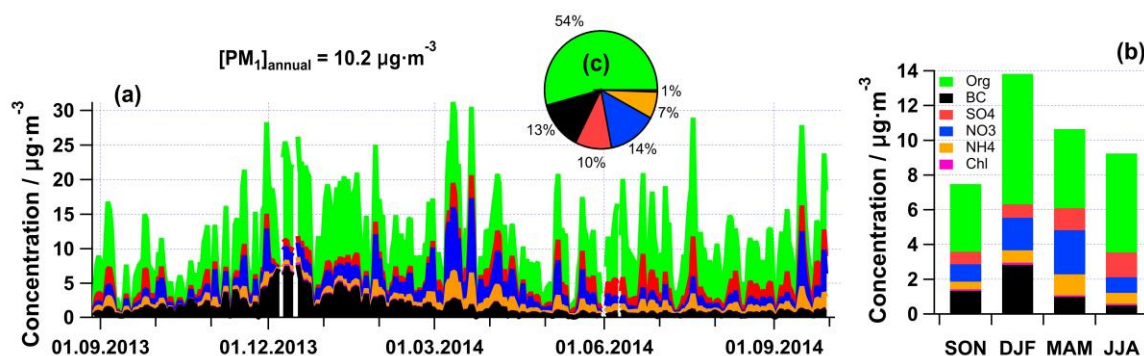


**Fig. 1** Chemical composition of PM<sub>1</sub> in Magadino 2013-2014 – daily (a), seasonal (b) and annual (c) averages. The labels indicate non-refractory organics (Org), sulphate (SO<sub>4</sub>), nitrate (NO<sub>3</sub>), ammonium (NH<sub>4</sub>) and chloride (Cl<sup>-</sup>) measured by the ACSM, and black carbon (BC) measured by light absorption.

Seasonally averaged diurnal cycles of NR-PM<sub>1</sub> components and eBC are displayed in **Fig. 2**. In this study, all the data is based on local time (Central European Time). In fall, spring and summer, the diurnals of these pollutants seem to be mainly affected by the development of the boundary layer height (BLH). Most of the species show similar diurnal trends for these three seasons. In addition, summer has the highest sulphate concentration due to the enhanced photochemical production. In winter, air pollutants are accumulated during the evening and night due to the thermal inversion. In general, eBC and organics have higher levels due to enhanced biomass burning emissions and a lower BLH. We observed distinct midday peaks of organics, sulphate, nitrate, ammonium, chloride, and NO<sub>x</sub> in the winter. Magadino experienced a series of windless, cold, but sunny periods from December 2013 to January 2014, including such sharp peaks (**Fig. S6a**). This was due to advection within the shallow boundary layer as both primary and secondary pollutants increased simultaneously. At the same time, the local

wind speed near the ground was very low. One potential explanation was that the locally and regionally induced orography influenced winds, including vertical diffusion processes, caused these delayed midday peaks. However, these processes remain difficult to track without spatially distributed measurements. Such phenomena were not observed during cloudy, cold, and windless days (**Fig. S6b**) without thermally induced meteorological processes. Unlike other seasons, the dilution process due to vertical mixing happened only after noon time due to strong inversions during the night and late irradiation of the valley surface in the winter.

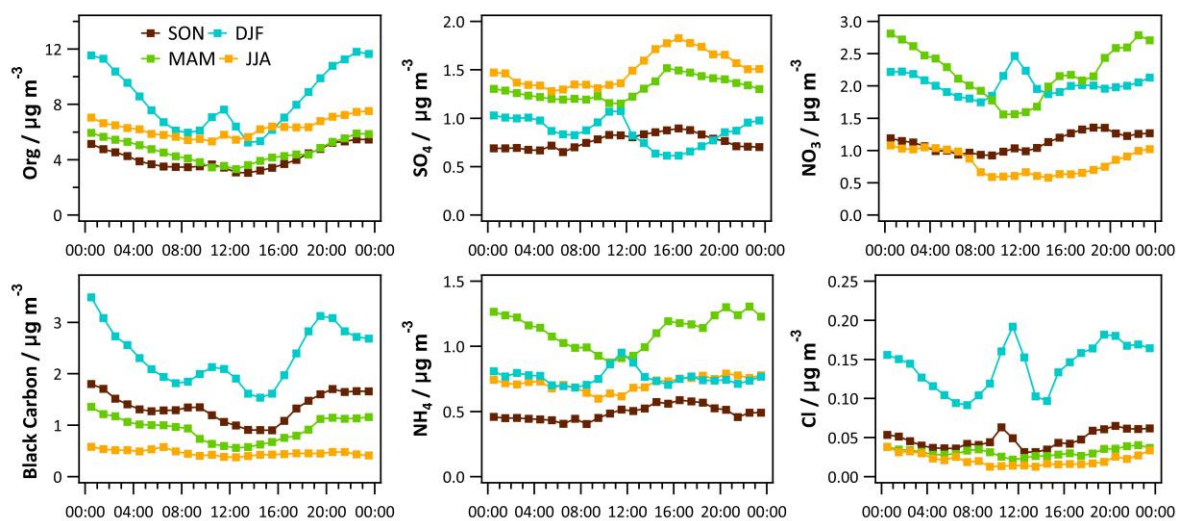


**Fig. 2** Seasonal, diurnal cycles of the measured  $PM_{10}$  components (hourly averages) for the organic and inorganic species (sulphate, nitrate, ammonium, and chloride) of the ACSM, and equivalent black carbon.

### 3.2 Seasonal PMF *Pre-tests*

The automated rolling PMF analysis requires the knowledge of the reference profiles as well as the number of factors. This section presents how the number of factors was determined based on seasonal PMF *pre-tests* (refer to Section 3.2.1 in the Supplement for methodology). Initially, unconstrained PMF (3 to 6 factors) was performed separately for the different seasons by

following the SA guidelines provided by Crippa et al. (2014). Typically, the HOA profile is characterised by a high contribution of alkyl fragments (*e.g.*  $m/z = 43$ ,  $m/z = 57$ ) and the corresponding alkenyl carbocations (*e.g.*  $m/z = 41$ ,  $m/z = 55$ ), and the factor profile is relatively consistent over time and different locations. The BBOA profile exhibits significant signals at  $m/z = 60$  and  $m/z = 73$ , which are well-known fragments arising from the fragmentation of anhydrous sugars present in biomass-related emissions (Alfarra et al., 2007). The HOA profile is present throughout the whole year for the unconstrained PMF runs, while the BBOA profile exists for all seasons except in summer. However, as shown in **Fig. S2**, the measured fraction of  $m/z = 60$  during summer was above the background level of  $0.3\% \pm 0.06\%$  for biomass burning-related air masses (Aiken et al., 2009; Cubison et al., 2011; DeCarlo et al., 2008). In addition, the scaled residual at  $m/z = 60$  was decreased when a BBOA factor profile was constrained. Thus, we decided to constrain the BBOA factor for all seasons to potentially capture local events, such as open fires and barbeques in summer.

No evidence for the presence of a cooking-related OA (COA) factor was found based on the seasonal pre-analysis of the key fragments ( $m/z = 55$  and  $m/z = 57$ ). **Figure S3** shows no difference in the slope of the absolute mass concentration of  $m/z = 55$  vs  $m/z = 57$  for different hours of the day (**Fig. S3a**), while different seasons show different slopes (**Fig. S3b**). Therefore, a COA factor was not considered in the PMF model. Moreover, a rapid increase of the measured fraction of  $m/z = 58$ ,  $84$ , and  $98$  together with  $m/z = 39$  (potassium signal) was observed after a filament exchange on 14 April, 2014. It was likely that the ACSM's sensitivity towards those ions was changed by the filament exchange. Also, this 58-OA factor was present for spring, summer, and autumn in 2014 in unconstrained PMF runs all the time after the filament change. Therefore, we kept this factor for these three seasons.

For the factor(s) with a secondary origin, we performed PMF models with a different number of factors (3–6) to assess if the oxygenated OA (OOA) factor is separable without mixing with primary organic aerosol (POA) factors (with a high contribution of  $m/z$  44 that is likely dominated by the  $\text{CO}_2^+$  ion, derived from decomposition of carboxylic acids (Duplissy et al., 2011)). We conducted these tests (with a different number of factors) independently for the different seasons (autumn 2013, winter, spring, summer, autumn 2014).

We analysed the winter data first by constraining an HOA factor profile (Crippa et al., 2013) with a tight  $a$ -value of 0.05. The 3-factor solution (with one OOA factor, i.e., less oxidised OOA (LO-OOA) and more oxidised OOA (MO-OOA)) showed similarly good agreement of HOA and BBOA with the external tracers ( $\text{NO}_x$ , eBC from traffic source (eBC<sub>tr</sub>), eBC from wood burning source (eBC<sub>wb</sub>)) as the 4-factor solution (with two OOA factors). However, the scaled residual of  $m/z$  60 was reduced for the solution with two OOA factors. Moreover, the solution with one OOA factor was not sufficient to explain the variabilities of measured  $f_{44}$  vs  $f_{43}$  (excluding the primary organic aerosol (POA) factors). For 5- and 6-factor solutions, the BBOA and LO-OOA factors started to split. Eventually, we selected the 4-factor solution (HOA, BBOA, MO-OOA, LO-OOA) as the best representation of the winter data.

After the bootstrap seasonal PMF runs of the winter data (details in Section 3.2.2 of the Supplement), we extracted the HOA and BBOA profiles to use them as the reference factor profiles (**Fig. S4**) for the *pre-tests* of other seasons. For the spring, summer, and autumn seasons, 3- to 6-factor PMF solutions were modelled separately for each season by constraining the HOA ( $a$ -value=0.1) and BBOA ( $a$ -value=0.3) profiles. For the 3-factor solution, we observed an OOA factor with some signals at  $m/z$  58, 84, and 98, which we could not relate to a specific source or process. Also, the scaled residuals of variables showed significant levels for these three ions. In addition, the time series and factor profile of 58-OA were so distinct that PMF

could easily resolve it. When we increased the number of OA factors from 3 to 4, a factor dominated by  $m/z$  58, 84, and 98 emerged, named 58-OA. However, the OOA factor still showed slight signals at  $m/z$  58, 84, and 98. An increase in the number of factors from 4 to 5 did not only result in a decrease in  $\frac{Q}{Q_{exp}}$ , but also in “clean” OOA factors without mixing with the 58-OA factor. A further increase in the number of factors did not change  $\frac{Q}{Q_{exp}}$  substantially ( $< 1\%$ ), and the sixth factor was a mathematical split of the 58-OA factor with  $m/z$  58 as the dominating variable. Thus, the 5-factor PMF model was chosen as the most appropriate for the spring, summer, and autumn 2014 to isolate this instrumental artefact via PMF. We did not add the 58-OA factor for the autumn season in 2013 since it appeared only after the filament exchange on 14 April 2014. This 58-OA factor was included while running PMF because of the rapid drop of the  $\frac{Q}{Q_{exp}}$  from 4 to 5 factors in the PMF model, but the source of this factor will not be discussed in the manuscript.

### 3.3 Full-year rolling PMF analysis

Here we present the optimised time window size (14 days) (details of the time window optimisation are given in Section 4 of the Supplement and in **Fig S10**). In total, we considered 53.4% of the PMF runs (11087 out of 20750) with only 11 non-modelled data points. The results of the full-year PMF analysis of the 30-min resolved ACSM data are summarised in **Fig. 3**. The relative contributions of the OA factors are in addition shown in **Fig. 3b**. The primary traffic-related HOA had tiny variation (seasonal averages between 8.1 and 10.1%) throughout the year (**Fig. 4**). In contrast, BBOA showed a distinct yearly cycle (8.3–27.4%) with a yearly averaged contribution of 17.1%. It increased significantly (to 27.4%) in winter which is typical for Alpine valleys (Szidat et al., 2007). It means that biomass burning was the most important primary OA source during the cold season in Magadino. The  $eBC_{wb}$  showed similar trends as the BBOA factor time series during the cold seasons (**Fig. 3c**). The



contribution of 58-OA remained small before the filament was changed on 14 April 2014, which is expected because we could not retrieve this factor in seasonal unconstrained PMF runs before April 2014.

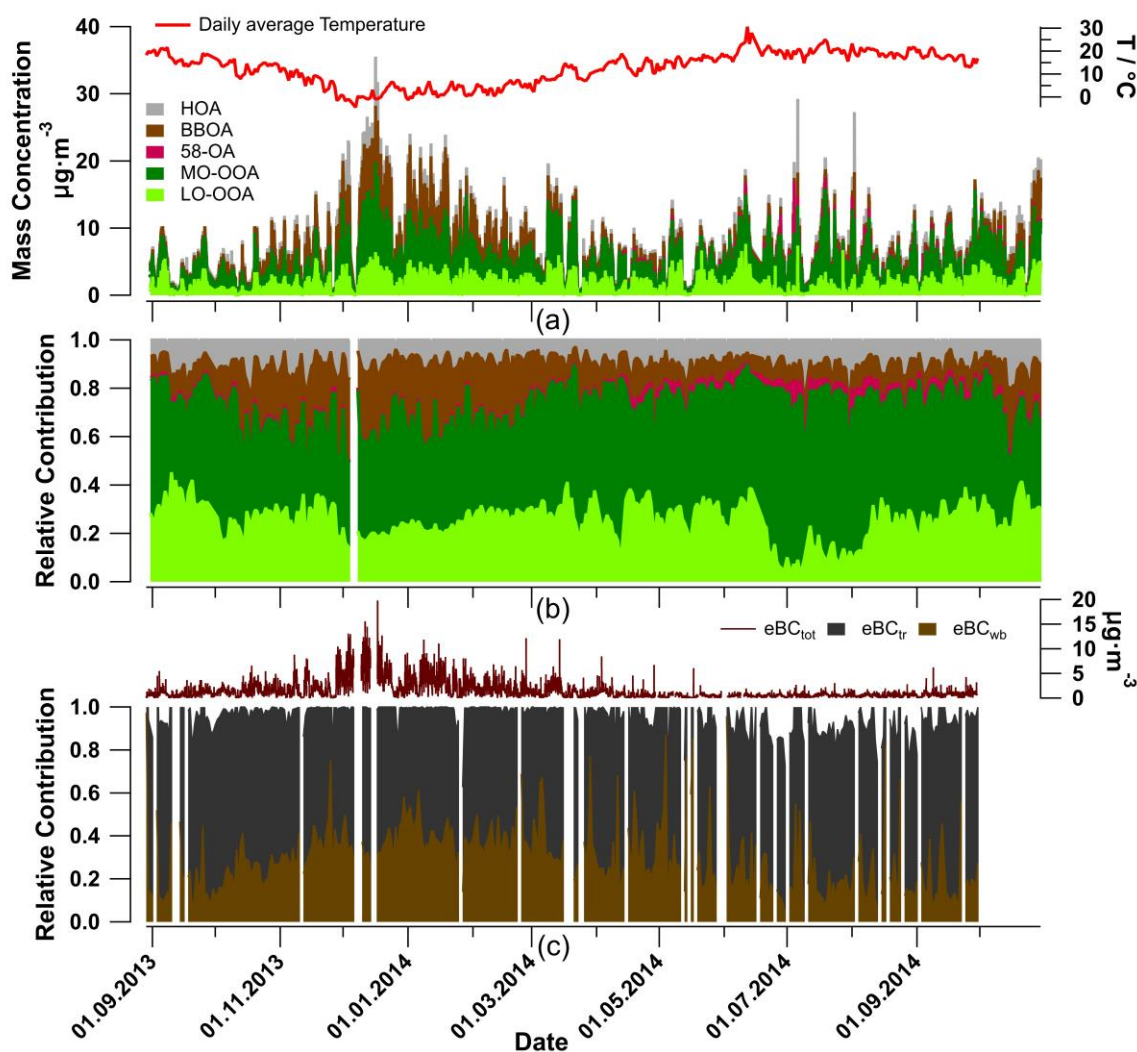


**Fig. 3** Annual cycles of OA components: (a) absolute and (b) relative OA contributions plotted as 30-min resolved time series, (c) BC source apportionment.

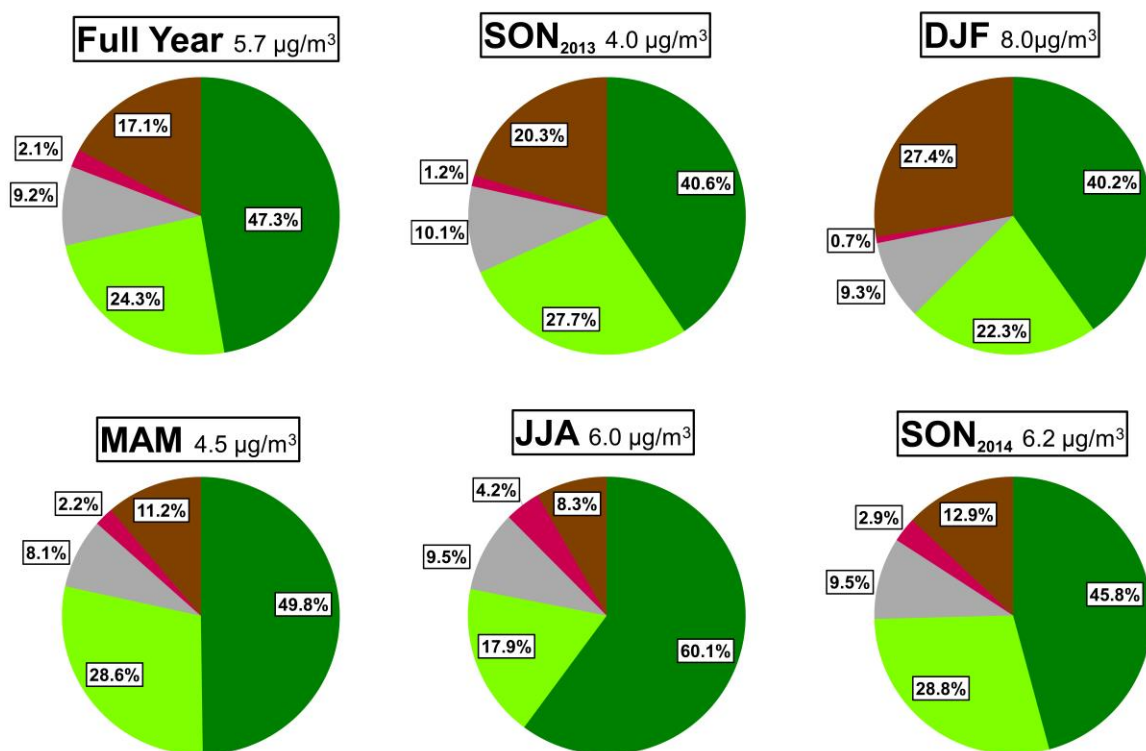


**Fig. 4** OA pie charts for the whole year and for the different seasons.

In this study, we retrieved two OOA factors, LO-OOA and MO-OOA. Total OOA (LO-OOA+MO-OOA) contributed substantially to the total OA mass throughout the whole year, with an average contribution of 71.6% (**Fig. 3b**; **Fig. 4**). In general, the contribution of OOA to the total OA mass did not vary distinctly over the seasons but reached a maximum of 90.1% on 12 June 2014, the day with the highest daily average temperature (30.7 °C).

In this work, we made head-to-head comparisons between the seasonal bootstrap solutions and the rolling PMF results (see **Fig. A1**, **Fig. A2**, **Fig. A3**, and **Table A1** in the Appendix) in terms of mass concentrations, factor profiles, scaled residuals, and correlations between time series for each factor and corresponding external tracers. We found consistent factor profiles and mass concentrations for the constrained factors (i.e., HOA, BBOA, and 58-OA), while OOA factors showed quite some differences in both mass concentrations and factor profiles. Rolling

PMF provided slightly better correlations and smaller scaled residuals. Therefore, we consider rolling PMF results to be more environmentally reasonable than those of the seasonal PMF (more details in Appendix A).

### 3.3.1 Optimised OA factors retrieved from a rolling PMF model

The primary and secondary OA factors retrieved as an annual mean of all optimised PMF solutions together with their diurnal cycles for all seasons are shown in **Fig. 5**. Note that the primary factors (HOA, BBOA, and 58-OA) were constrained, where the 58-OA profile was tightly constrained with an  $\alpha$ -value of 0.05 due to the uniqueness of its chemical profile, while the HOA and BBOA model profiles varied more due to looser constraints (**Fig. S8**). HOA and BBOA had averaged  $\alpha$ -values of  $0.207 \pm 0.036$  and  $0.195 \pm 0.050$ , respectively. In addition, they both showed good agreement with previous studies (Crippa et al., 2014; Ng et al., 2011b). The probability distribution function (PDF) of applied  $\alpha$ -values for selected PMF runs vs time was also investigated (**Fig. S8**). Most selected runs chose  $\alpha$ -values of 0.1–0.3 for HOA and BBOA. The OOA factors show more significant variations in the chemical profiles because these two factors were not constrained due to the high variability of oxidation processes governing the secondary factors.

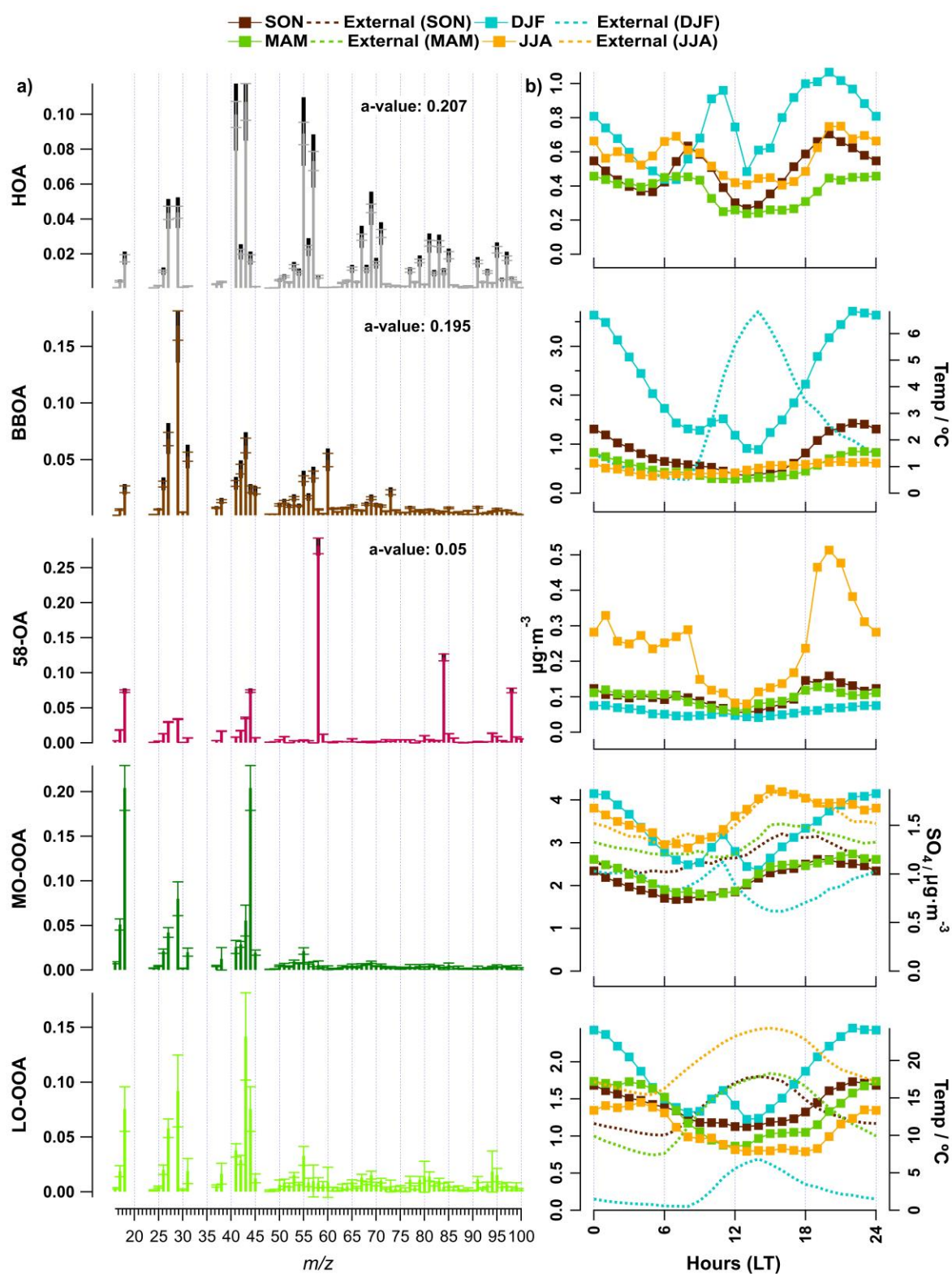


**Fig. 5** Overview of the primary and secondary OA components in Magadino in 2013-2014: (a) OA factor profiles and (b) seasonal diurnal cycles of HOA, BBOA, 58-OA, MO-OOA, and LO-OOA. The ambient temperature is shown on the LO-OOA diurnal plots. In (a) the error bar is the standard deviation; the black bars show the maximum and the minimum that the variable was allowed to vary from the reference profiles. The average, 10<sup>th</sup>, and 90<sup>th</sup> percentiles for a-

values of HOA are 0.195, 0.007 and 0.378, respectively. Also, the average, 10<sup>th</sup>, and 90<sup>th</sup> percentiles for a-values of BBOA are 0.202, 0.025 and 0.379, respectively.

Due to extensive residential wood combustion combined with winter inversions, the concentrations of BBOA and eBC<sub>wb</sub> were three times higher at night than at midday. As discussed above, during winter, all of the air pollutants, including all PMF factors peaked concurrently at 10–11 a.m. (local time) due to delayed illumination of the valley site and slow wind speed near the ground (light blue markers in **Fig. 2** for total PM<sub>1</sub> and **Fig. 5b**). In summer, an additional local photochemical production led to an increasing MO-OOA mass during the day (red markers in **Fig. 5b**), similar to the sulphate diurnal behaviour ( $R^2=0.63$ ). A nighttime increase and a daytime decrease of the LO-OOA mass during spring and summer apparently followed condensation and re-evaporation cycles of semi-volatile species, similar to the behaviour of ammonium nitrate. Additionally, nocturnal chemistry of NO<sub>3</sub>/N<sub>2</sub>O<sub>5</sub> radicals could lead to the formation of HNO<sub>3</sub> *via* N<sub>2</sub>O<sub>5</sub> hydrolysis and of organic nitrates *via* oxidation of VOCs (Brown et al., 2004; Dentener and Crutzen, 1993), thus influencing the diurnal cycles of both particulate nitrate and LO-OOA (with  $R^2 = 0.48$  for spring and  $R^2 = 0.36$  for summer).

**Figure 6** also presents the diurnal cycles of HOA, eBC<sub>tr</sub> and NO<sub>x</sub> with different patterns for weekdays and weekends. The hourly averages of HOA and eBC<sub>tr</sub> and the NO<sub>x</sub> mixing ratio peak during the morning and evening rush hours over the weekdays, while on the weekends, there is only an evening pollution increase coinciding with the time when people come back from holidays or nighttime leisure activities.

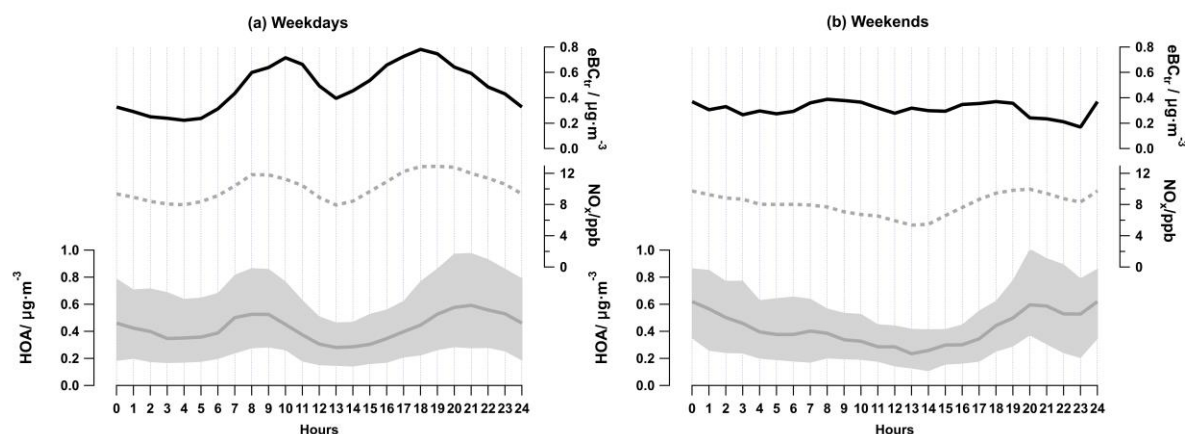


**Fig. 6** Diurnal cycles of HOA (grey symbols), black carbon apportioned to traffic emissions  $eBC_{tr}$  (dashed lines) and  $NO_x$  (dotted lines) for weekdays (a) and weekends (b). The shaded areas represent the interquartile range for HOA (1-hour averages).

### 3.3.2 $f_{44}/f_{43}$ analysis of secondary OA factors

While  $m/z$  44 is mostly from the fragment of  $CO_2^+$ , a fingerprint of oxygenated species,  $m/z$  43 can originate from  $C_2H_3O^+$  (a fingerprint of semi-volatile species) or  $C_3H_7^+$  (a fingerprint of the primary emissions of hydrocarbon-like species) (Canonaco et al., 2015; Chirico et al., 2010; Ng et al., 2010). Thus,  $f_{44}$  and  $f_{43}$  are often used to identify the oxidation state of the factors, which is crucial to differentiate the MO-OOA and LO-OOA factors. Under the premise that the POA factors and the 58-OA factor are all well-resolved, it is essential to investigate the relationship between the  $m/z$  44 and  $m/z$  43 signals in the OOA factors to determine whether or not one/two OOA factors are sufficient to explain the dataset. In addition, the shapes of the yellow-red dots shown in an  $f_{44}$  vs  $f_{43}$  plot (**Fig. 7**) may also include some source-related information. **Figure 7** depicts the relationship between  $f_{44}$  and  $f_{43}$  of two modelled OOA factors for the different seasons. The yellow cloud of data points represents the measured  $f_{44}$  vs  $f_{43}$  after subtracting the  $m/z$  44 and  $m/z$  43 signals contributed by the primary HOA, BBOA and 58-OA factors (Eq. S11 and Eq. S12). They are colour coded by the total OA mass concentration (data points with OA mass concentration below  $2 \mu g \cdot m^{-3}$  are hidden).



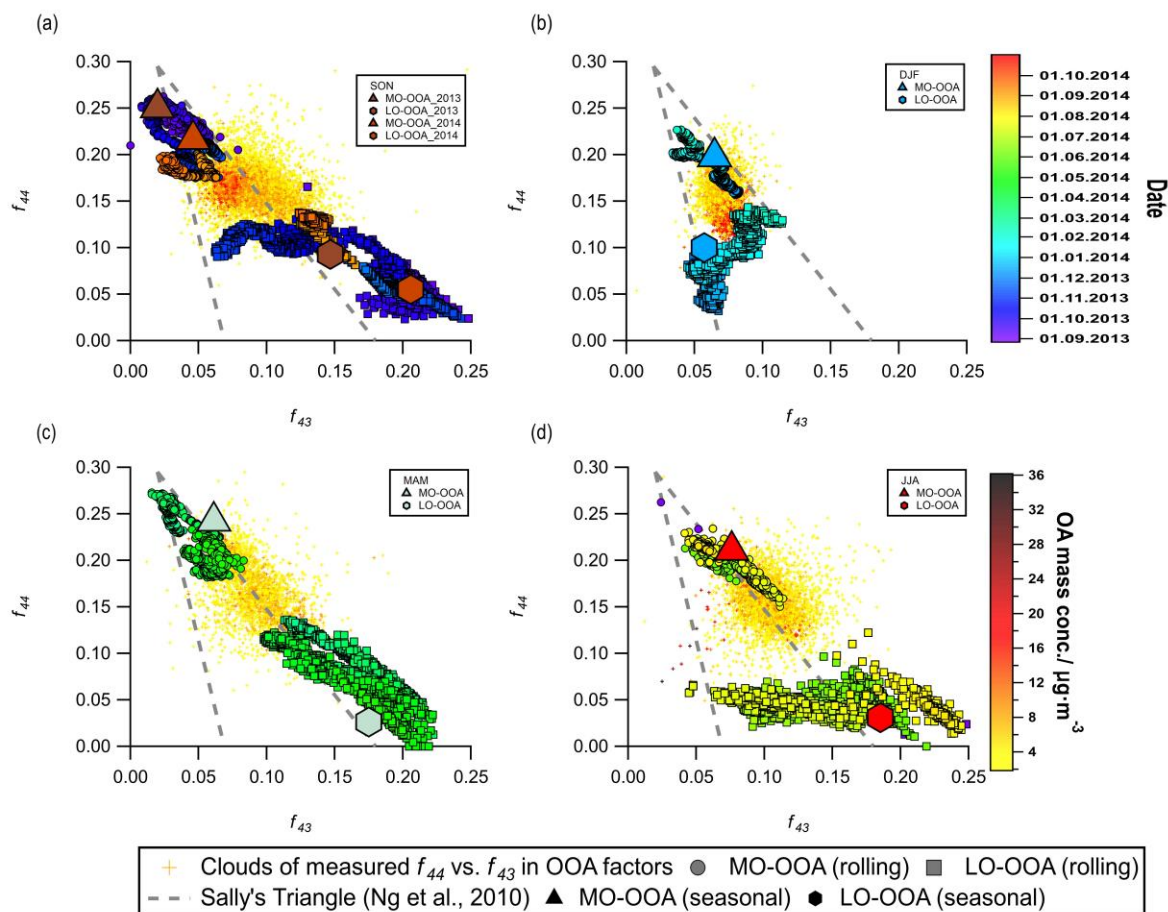


**Fig. 7**  $f_{44}$  and  $f_{43}$  of OOA (after subtraction of signals contributed by the primary HOA, BBOA and 58-OA factors) for four different seasons. The small yellow/red crosses of data points represent the  $f_{44}$  vs  $f_{43}$ . They are colour-coded by the total OA mass concentration. The bigger size of triangles and hexagons represent the ratios between  $f_{44}$  and  $f_{43}$  intensities within the factor profiles of MO-OOA and LO-OOA in seasonal solutions, respectively. The smaller size of circles and squares are ratios between  $f_{44}$  and  $f_{43}$  intensities within the factor profiles of MO-OOA and LO-OOA from rolling PMF analysis, which are colour-coded by date and time. The dashed lines represent Sally's triangle from Ng et al., (2010) and depict the region where OOA from multiple PMF analyses during the last decade resided in the  $f_{44}$  vs  $f_{43}$  space.

As shown in **Fig. 7a**, the data points in Sep–Oct (both in 2013 and 2014) were located on the right side of the triangle presented first by Ng et al. (2010), while the November (2013) data points were located within the triangle. In addition, the spring and summer data points (**Fig. 7c** and **Fig. 7d**) were all located rather on the right side of the triangle, but the winter points lied within the triangle (**Fig. 7b**). We made a similar plot but with monthly resolution and different colour codes in **Fig. S9**. The data points located within the triangle correspond to the time with

a lower temperature than those that are closer to the right side of the triangle in **Fig. S9**. It could be explained by the increased biogenic OOA contributions when the temperature was higher, as biogenic OOA tends to be distributed along the right side of the triangle (Canonaco et al., 2015; Pfaffenberger et al., 2013). Also, when the temperature decreases, the increased biomass emissions make the OOA points lie vertically within the triangle (Canonaco et al., 2015; Heringa et al., 2011), which is the case for the winter data (**Fig. 7b**).

In July 2014, the rolling PMF LO-OOA moved towards the left side of the plot due to increasing influences from  $m/z$  80,  $m/z$  94 ( $C_2H_6S_2^+$ ),  $m/z$  95, and  $m/z$  96 (**Fig. S7**). Because the OA signal of  $m/z$  80 is directly calculated from  $m/z$  94 (Allan et al., 2004), we did not investigate the sources of  $m/z$  80. In July, a potential source of these distinct ions was some oxidation products of dimethyl disulphide, which shows signals at  $m/z$  94,  $m/z$  95, and  $m/z$  96 (NIST Mass Spectrometry Data Center, 2014). Dimethyl disulphide is widely used in pesticides. Considering that the sampling site is in the middle of a farmland, and the diurnal variation of  $m/z$  94 appeared to peak during the daytime, we considered the LO-OOA in July to be highly affected by agricultural activities. However, the static factor profiles of summer LO-OOA from the seasonal summer solution had much smaller intensities for  $m/z$  80 and  $m/z$  94 (**Fig. S4**), which enhanced the scaled residuals for these two variables in the seasonal solutions.

In winter, LO-OOA (**Fig. 9b**) was highly affected by biomass burning emissions characterised by the presence of  $m/z$  60, 73 (Alfarra et al., 2007), and the LO-OOA position in the  $f_{44}$  vs  $f_{43}$  space moved towards the top-right direction in the plot due to the increasing biogenic influence as the temperature rose (**Fig. 7b, Fig. S9**) (Canonaco et al., 2015).

**Figure 7** also highlights the advantages of rolling PMF over seasonal PMF due to its time-dependent source profiles. Both seasonal and rolling results show that the linear combinations of OOA factors could adequately explain most of the measured OOA points for all the seasons.

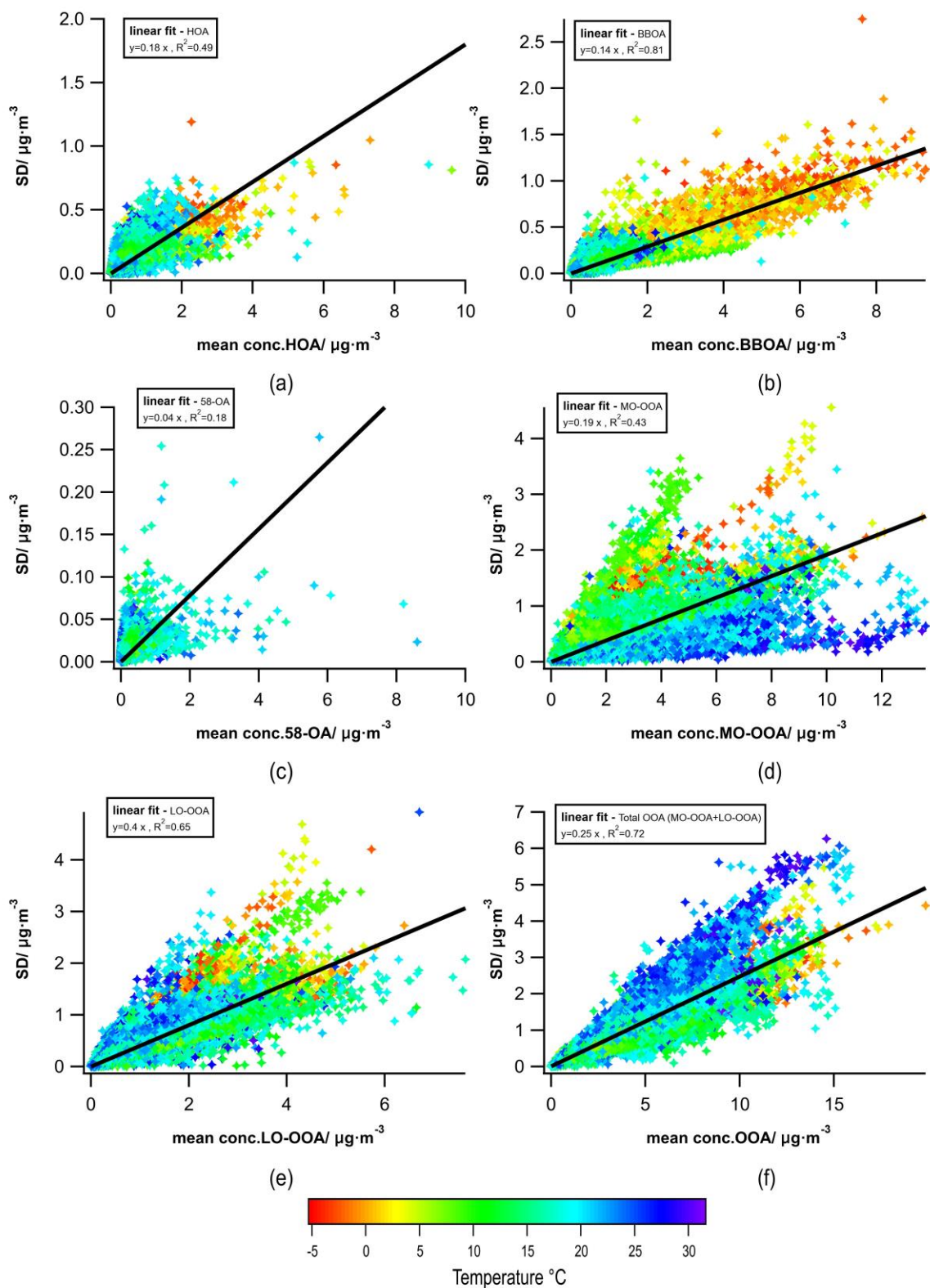


However, with the static OOA factors for seasonal PMF solutions, it remains challenging to capture the variabilities of some measured data points. In contrast, the rolling PMF OOA factors can move correspondingly with the temporal changes of the clouds, which moves the factor profiles closer to reality and potentially decreases the scaled residuals significantly (**Fig. A3**). **Figure S9** also shows the movements of LO-OOA and MO-OOA factor profiles monthly, where LO-OOA moves towards the right direction as the temperature increases, except for the two light blue squares (June and July) in **Fig. S9a**. It is clear that temperature plays an important role for the positions of LO-OOA and MO-OOA in the  $f_{44}$  vs  $f_{43}$  space due to its influences on the OOA sources (biogenic or anthropogenic) as well as the atmospheric processes, which is consistent with previous studies in Zurich (Canonaco et al., 2015).

### 3.3.3 Statistical and rotational uncertainties

As suggested by Canonaco et al. (2021), combining the bootstrap resampling and the random  $\alpha$ -value techniques together with the rolling mechanism, we calculated the standard deviation ( $\sigma$ ) and the mean ( $\mu$ ) of the mass concentration for each data point from each OA factor in selected “good” PMF runs. We estimated the uncertainty of each OA factor using the slope of the linear fit of  $\sigma$  vs  $\mu$ . (**Fig. 8**). Since the 58-OA factor was tightly constrained with an  $\alpha$ -value of 0.05, it had the smallest variability (4%). Overall, we found relatively smaller errors of HOA, BBOA, and MO-OOA (i.e., 18%, 14%, and 19%, respectively) and an error of 25% for LO-OOA, which is comparable with the previous study (Canonaco et al., 2021). The errors for both the MO-OOA and the LO-OOA factor showed some temperature dependence. However, this actually varied with time, and the errors did not significantly change when we divided the dataset into four different temperature groups. Still, data points with higher temperature tended to have larger error for the total OOA than with lower temperature (**Fig. 8f**). This was most likely due to the increase of biogenic emissions and the increasing photochemistry (high  $O_3$

515 and NO<sub>2</sub> concentration) at high temperatures (>20 °C), which caused the complexity of the  
516 OOA sources.



517

518 **Fig. 8** Absolute statistical uncertainties of PMF for HOA, BBOA, 58-OA, LO-OOA, MO-OOA  
 519 and total OOA (LO-OOA+MO-OOA) for all data. The data points are colour-coded by  
 520 temperature. The PMF error (uncertainties) of selected PMF runs and rotational uncertainties  
 521 are estimated using the slope of the linear regression of standard deviation ( $\sigma$ ) vs. the averaged  
 522 mass concentration ( $\mu$ ) for each factor.

523

### 524 3.3.4 Online vs. offline

525 The mass concentrations for HOA, BBOA and total OOA were compared with corresponding  
526 offline AMS results (Vlachou et al., 2018) (**Fig. S11**). Despite some disagreement during  
527 winter (BBOA and total OOA), BBOA showed a high correlation –with the offline results for  
528 both PM<sub>10</sub> and PM<sub>2.5</sub>, with  $R^2$  of 0.83 and 0.84, respectively. The correlation for total OOA  
529 was somehow lower, with  $R^2$  of 0.31 and 0.46 for the offline results of PM<sub>10</sub> and PM<sub>2.5</sub> OOA,  
530 respectively. **Figure 9a** shows that the rolling results had a higher OOA concentration during  
531 the winter season than the offline PM<sub>2.5</sub>/PM<sub>10</sub> results, while the rolling results present a lower  
532 BBOA concentration during the winter season than the offline PM<sub>2.5</sub>/PM<sub>10</sub> results (**Fig. S11b**).  
533 As shown in **Fig. 9b**, LO-OOA in the rolling results were heavily affected by biomass burning  
534 with apparent biomass trace ions (i.e.,  $m/z$  60 and 73). The offline results apportioned this  
535 biomass burning-affected LO-OOA to BBOA, whereas the online ACSM measurements with  
536 a higher time resolution could capture the fast oxidation process of biomass burning sources.  
537 In addition, the rolling PMF technique enabled the LO-OOA factor profile to adapt to the  
538 temporal viabilities of OA sources, so the relatively aged biomass burning OA fraction was  
539 apportioned into LO-OOA during wintertime by rolling PMF. The yellow line in **Fig. 9a**  
540 depicts the mass concentration of  $m/z$  60 within LO-OOA, which clearly shows significant  
541 enhancements during winter and a good agreement with the total OOA time series from the  
542 rolling results. **Figure S11** shows that HOA did not correlate at all, which is expected because  
543 HOA is typically not water-soluble, and therefore has a very low recovery rate of 0.11 for the  
544 offline AMS technique based on the Daellenbach et al. (2016).

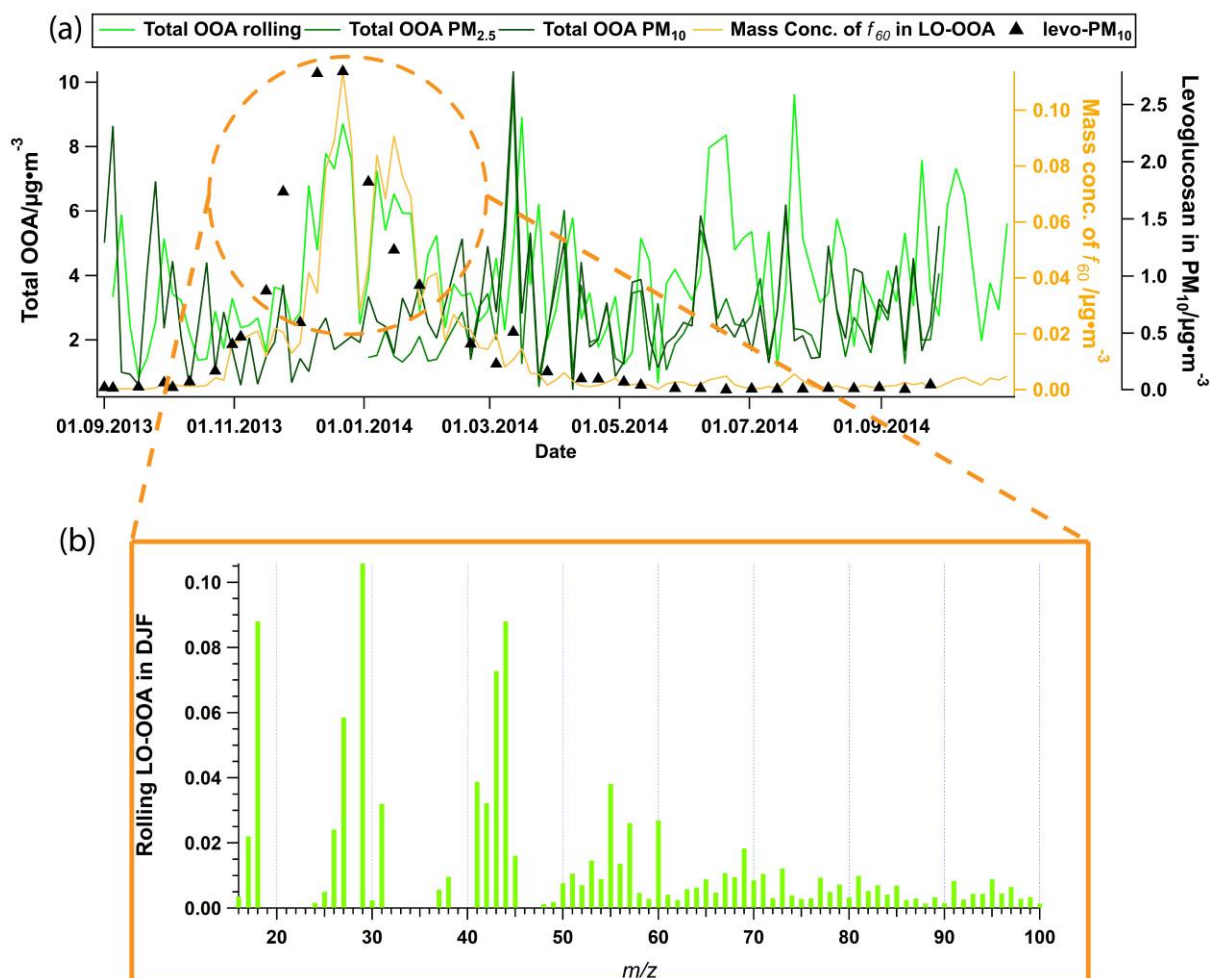


**Fig. 9** (a) Time series of total oxygenated organic aerosol (LO-OOA+MO-OOA) from online and offline source apportionment solutions, together with  $f_{60}$  in LO-OOA for online solution, and levoglucosan in PM<sub>10</sub> filters; (b) Averaged LO-OOA factor profile from the online solution during DJF (Dec, Jan, and Feb), when online total OOA is significantly higher than that of the offline solution.

## 4 Conclusions

In this study, we conducted the first rolling PMF analysis on a 13-month ACSM data collected at a rural site in Switzerland. With the help of the small rolling PMF time window and the random  $\alpha$ -value and bootstrap resampling analysis, we obtained a time dependent SA result with error estimations. Overall, we resolved a comprehensive 5-factor solution with HOA, BBOA, 58-OA, MO-OOA, and LO-OOA. The contribution of HOA was constant during the

year (8.1–10.1%), while BBOA showed a clear seasonal variation (8.3–27.4%), which peaked during winter (due to an increased residential heating source) and contributed least in summer. OOA was a dominant source throughout the year, with a contribution of 71.6% on a yearly average. However, the biomass burning source had a strong influence on LO-OOA formation in winter. Together with BBOA, they make residential heating a considerable source at Magadino during winter. Therefore, mitigation of residential wood combustion should be considered to reduce PM levels in Magadino and similar locations, especially in winter. Hüglin and Grange (2021) showed that the reduction of residence wood combustion has already shown some effects in PM mitigation in Magadino. However, the biomass burning contribution remains significant in this region.

This manuscript also provided a recommended criterion list (**Table S1**) and a novel way to define thresholds with minimum subjective judgements (student's *t*-test), which could be a leading example for other SoFi Pro users to conduct rolling PMF. To ensure a good representation of the modelled POA factors and to validate the SA results, we also used the correlations between the PMF factor time series and external data. Both HOA and BBOA agreed well with the corresponding external tracers ( $\text{NO}_x$ ,  $\text{eBC}_{\text{tr}}$ , and  $\text{eBC}_{\text{wb}}$ ) for the yearly cycles, except for summer. This is because the aethalometer model for  $\text{eBC}$  SA has higher uncertainties with smaller  $\text{eBC}_{\text{wb}}$  mass concentrations. Also,  $\text{NO}_x$  could originate from multiple sources in this season. Therefore, we used HOA vs  $\text{eBC}$  and  $EV_{60,\text{BBOA}}$  to justify these two factors in summer. The correlation of HOA vs  $\text{eBC}$  had an  $R^2$  of 0.28, with an  $EV_{60,\text{BBOA}}$  of 0.55 in summer. Moreover, the MO-OOA and LO-OOA factors were well correlated with inorganic  $\text{SO}_4$  and  $\text{NO}_3$ , respectively. The identified primary and secondary OA factor profiles were consistent with the OA factors previously found at various urban, rural, and remote European locations.

This paper assessed the statistical and rotational uncertainties of the PMF solution by combining the bootstrap resampling technique and the random  $\alpha$ -value approach. It shows relatively small errors for constrained factors compared with a previous study in Zurich (Canonaco et al., 2021) and comparable errors for the OOA factors.

We also presented a head-to-head comparison between seasonal PMF solutions and the rolling PMF solution. The POA factors showed good agreement between seasonal and rolling PMF solution, while the OOA factors exhibited greater differences. Overall, the rolling PMF provided slightly better agreements with external tracers, especially between the OOA factors and corresponding inorganic salts. In addition, the rolling PMF results provided a better representation of the measurements by adapting the temporal variations of OOA factors in the  $f_{44}$  vs  $f_{43}$  space, which also led to much smaller scaled residuals than for the seasonal PMF. Therefore, the rolling PMF is highly useful when the user wishes to better separate OOA factors (especially during cold seasons) and better represent the measurements. In addition, we will also recommend using the rolling PMF to facilitate the analysis of long-term trends of OA sources with some prior knowledge of OA sources. However, it remains challenging to objectively define the transition point to an improved source apportionment for rolling PMF analysis when a different number of OA factors is necessary for different periods. An upcoming manuscript (Via et al., in prep.) will present more details of the comparison between rolling and seasonal results for multiple datasets. The time series of BBOA and total OOA agreed well with those from offline AMS SA results (Vlachou et al., 2018), except for winter when the offline AMS technique did not capture the fast oxidation processes of biomass burning emissions.

Knowledge of diurnal, seasonal and annual changes in OA sources is essential for interpreting the yearly cycles of OA and defining mitigation strategies for air quality. With the help of more accurate and realistic OA sources, together with an estimation of the statistical uncertainty of

607 PMF, more constraints can be provided both for climate and air quality models. These  
608 improved results are therefore highly valuable for policymakers to solve aerosol-related  
609 environmental issues.

610



## 5 Appendix A: Comparison between seasonal and rolling PMF solutions

The bootstrapped seasonal PMF solutions were compared with the full-year rolling PMF results as follows. The correlations with external data, the ion intensities in the factor profiles and the mass concentrations retrieved from the two different source apportionment techniques were compared for each factor. The correlations of the factor time series with external data (i.e.,  $\text{NO}_x$ ,  $\text{eBC}_{\text{tr}}$ ,  $\text{eBC}_{\text{wb}}$ ,  $\text{eBC}_{\text{total}}$ ,  $\text{SO}_4$ ,  $\text{NO}_3$ , and  $\text{NH}_4$ ) are presented in **Table A1**. The rolling results generally showed slightly better correlations between LO-OOA and  $\text{NO}_3$ , MO-OOA and  $\text{SO}_4$ , and total OOA with  $\text{NH}_4$  than the seasonal PMF results, which is consistent with the comparison results from Canonaco et al. (2021). A significant improvement was evident for LO-OOA vs  $\text{NO}_3$  in spring (with  $R^2$  increasing from 0.02 to 0.48). Concerning the correlations of POA factors with external data, rolling results and seasonal showed similar results

**Table A1** Correlation coefficients ( $R^2_{\text{pearson}}$ ) between the factor contributions and expected tracers over the year and for individual meteorological seasons ( $p < 0.05$ ).

Factor	Yearly		SON_2013		DJF		MAM		JJA		SON_2014	
	Seasonal	Rolling	Seasonal	Rolling	Seasonal	Rolling	Seasonal	Rolling	Seasonal	Rolling	Seasonal	Rolling
HOA / $\text{NO}_x$	0.37	0.35	0.52	0.5	0.46	0.47	0.34	0.36	0.15	0.15	0.44	0.42
HOA / $\text{eBC}_{\text{tr}}$	0.34	0.33	0.29	0.35	0.41	0.42	0.39	0.31	N/A	N/A	0.38	0.39
HOA / $\text{eBC}$	0.55	0.51	0.79	0.77	0.77	0.73	0.5	0.41	0.29	0.28	0.5	0.47
BBOA / $\text{eBC}_{\text{wb}}$	0.82	0.82	0.81	0.79	0.84	0.81	0.67	0.6	N/A	N/A	0.3	0.27
MO-OOA / $\text{SO}_4^{2-}$	0.58	0.49	0.49	0.61	0.52	0.49	0.62	0.66	0.63	0.57	0.43	0.46
LO-OOA / $\text{NO}_3^-$	0.11	0.32	0.28	0.42	0.28	0.23	0.02	0.48	0.33	0.36	0.19	0.29
OOA / $\text{NH}_4^+$	0.46	0.44	0.52	0.55	0.34	0.26	0.73	0.75	0.48	0.47	0.57	0.59

**Fig. A1** showed a good agreement for two techniques, except for MO-OOA and LO-OOA. In general, the slope of 1.09 for rolling total OOA vs seasonal OOA suggests the seasonal PMF method tends to apportion more OOA components, while the slope ( $< 1$ ) for HOA and BBOA suggests that the seasonal PMF technique tends to apportion less HOA and BBOA. In addition,

58-OA shows the best agreement between the seasonal and rolling solutions due to the tight constraint of 58-OA with an  $a$ -value of 0.05.

The LO-OOA and MO-OOA factors showed worse agreement than the POA factors for the whole dataset. They had good correlations in each meteorological season, however, with different slopes. For instance, seasonal PMF underestimated LO-OOA in spring and fall 2014, but both seasons showed a high correlation with rather narrow scattering. The over-apportionment of MO-OOA compensated the under-apportionment of LO-OOA by seasonal PMF for these two seasons. Therefore, the summed OOA still showed a high correlation between rolling and seasonal PMF results. This is expected, as the rolling PMF allows the source profiles to adapt to temporal variations, while seasonal PMF only has static source profiles.

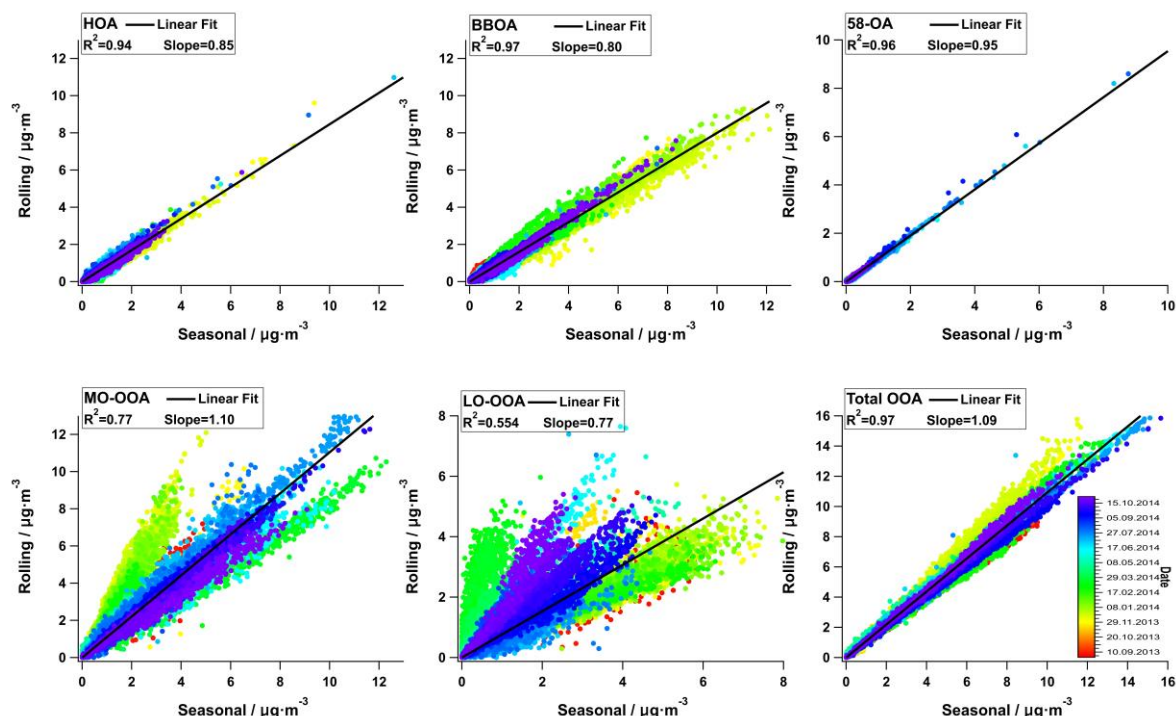


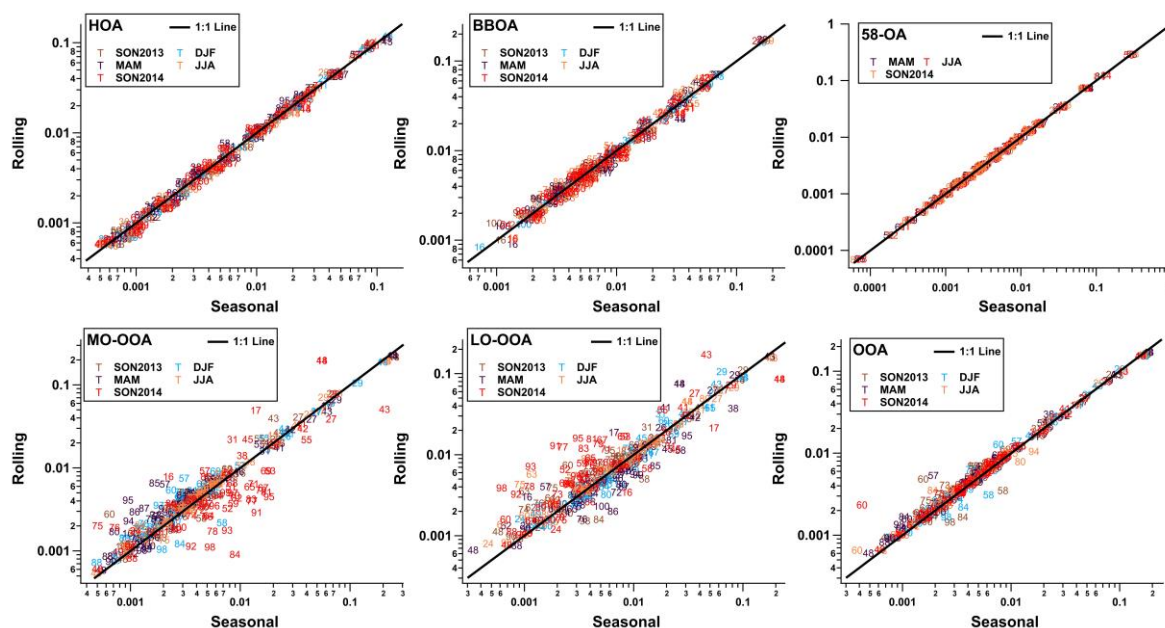
**Fig. A1** Comparison of the mass concentrations resulting from rolling PMF and from the seasonal analysis for each factor (colour coded by date and time).

645

646 The differences in the major variables of the OOA factors (i.e.,  $m/z$  44, 43, and 60) shifted the  
647 mass concentrations significantly. Therefore, we also compared the factor profiles for both  
648 techniques (**Fig. A2**). For instance, LO-OOA during spring showed higher intensity at  $m/z$  44  
649 for the rolling PMF results than for the seasonal PMF results (**Fig. A2**), which caused the  
650 underestimation of LO-OOA for the seasonal PMF in spring. When we averaged the total OOA  
651 factor using mass-weighted MO-OOA and LO-OOA factors, rolling PMF yielded higher  $m/z$   
652 60 for all seasons. As a result, seasonal PMF apportions slightly less summed OOA factors by  
653 around 9%, while apportions slightly more POA factors within 6%.

654 The profiles of the constrained factors (HOA, BBOA, 58-OA) from the rolling results show a  
655 very high correlation with the seasonal results (**Fig. A2**), which suggests that the primary  
656 factors and the tightly constrained factor (58-OA) were consistent with the static profiles from  
657 the seasonal PMF analysis.

658

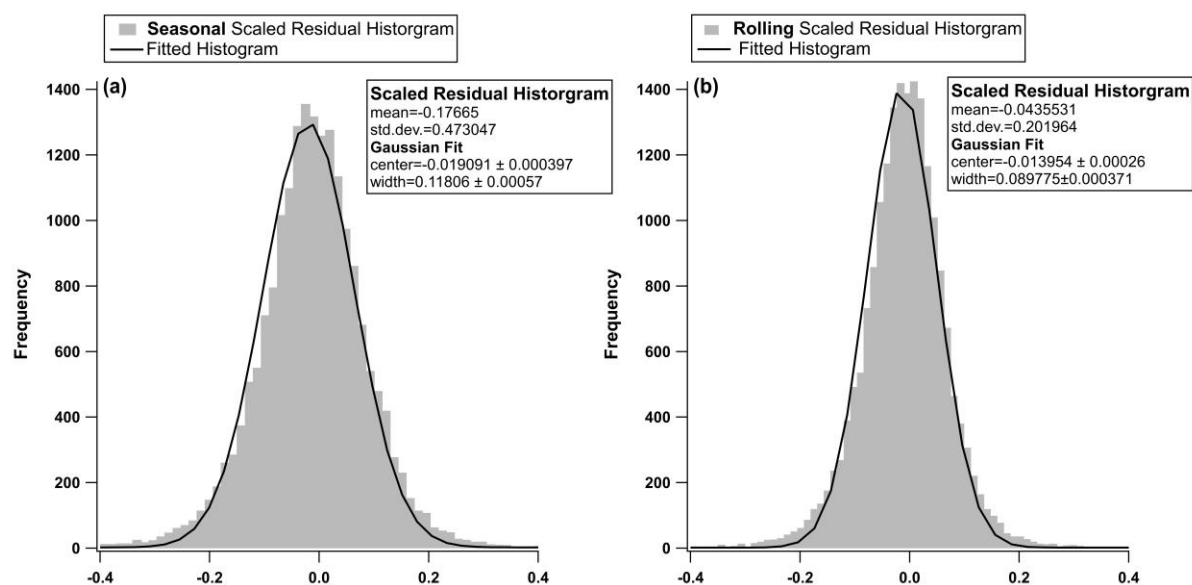


659

660 **Fig. A2** Profile comparisons between rolling results and seasonal results for each factor (log  
661 scale).

662

663 We compared the scaled residuals from both source apportionment techniques (**Fig. A3**). The  
664 rolling PMF solution had smaller scaled residuals (narrower histogram and the centre was  
665 closer to 0) than that of the seasonal PMF solution, which is expected because rolling PMF had  
666 more flexibility to adapt to the temporal variabilities of the OA sources.



668

669 **Fig. A3** Distribution of the scaled residuals over the whole year for the seasonal solution (a)  
 670 and the rolling solution (b).

671

672 Summarising, HOA and BBOA were consistent for rolling and seasonal PMF analysis in terms  
 673 of the time series, correlations with external tracers, and factor profiles due to the consistency  
 674 of their chemical factor profiles. In contrast, the MO-OOA and LO-OOA factors were more  
 675 scattered in averaged factor profiles and mass concentration, suggesting that seasonal PMF  
 676 analysis was insufficient to capture these temporal variations of their oxidation processes. Also,  
 677 rolling PMF showed smaller scaled residuals. Therefore, we conclude that the rolling PMF  
 678 analysis provides more realistic results than the seasonal analysis.

## 679 Data Availability

680 Data related to this manuscript are available at <https://zenodo.org/record/5113896> (Chen et al.,  
 681 2021).

## **Competing interests**

Y. S., F. C., A. T. K., C. B. are working for Datalystica Ltd., the company that developed the SoFi Pro software. All authors declare no competing interests in any form for this work.

## **Author contributions**

G. C. analysed the ACSM and BC data, then performed the rolling source apportionment and wrote the manuscript. Y. S. wrote the preliminary manuscript and analysed preliminary results. G. C., Y. S., F. C., A. T., K. R. D., J. G. S., I. El. H., U. B., and A. S. H. P. helped editing and reviewing the manuscript. Y. S, R. F. and P. G. helped to run the campaign. P. G., and C. H. provided external data to validate PMF solution. F.C. provided technique support for SoFi Pro. F.C., A. T., K. R. D., A. V., J. G. S., I. El. H., U. B., and A. S. H. P. participated in discussions for this study.

## **Acknowledgements**

The ACSM measurements were supported by the Swiss Federal Office for the Environment (FOEN). The leading role of the Environmental group of the Swiss Federal Laboratories for Materials and Testing (Empa) in supporting the measurements is very much appreciated. Y. S. acknowledges supports by the “Wiedereinsteigerinnen Program” at the Paul Scherrer Institute. This study was also supported by the cost action of Chemical On-Line cOmpoSition and Source Apportionment of fine aerosol (COLOSSAL, CA16109), a COST related project of the Swiss National Science Foundation, Source apportionment using long-term Aerosol Mass Spectrometry and Aethalometer Measurements (SAMSAM, IZCOZ0\_177063), as well as the EU Horizon 2020 Framework Programme via the ERA-PLANET project SMURBS (grant agreement no. 689443).

## References

- Aiken, A. C., Salcedo, D., Cubison, M. J., Huffman, J. A., DeCarlo, P. F., Ulbrich, I. M., Docherty, K. S., Sueper, D., Kimmel, J. R., Worsnop, D. R., Trimborn, A., Northway, M., Stone, E. A., Schauer, J. J., Volkamer, R. M., Fortner, E., de Foy, B., Wang, J., Laskin, A., Shutthanandan, V., Zheng, J., Zhang, R., Gaffney, J., Marley, N. A., Paredes-Miranda, G., Arnott, W. P., Molina, L. T., Sosa, G. and Jimenez, J. L.: Mexico City aerosol analysis during MILAGRO using high resolution aerosol mass spectrometry at the urban supersite (T0) – Part 1: Fine particle composition and organic source apportionment, *Atmos. Chem. Phys.*, 9(17), 6633–6653, doi:10.5194/acp-9-6633-2009, 2009.
- Alfarra, M. R., Prevot, A. S. H., Szidat, S., Sandradewi, J., Weimer, S., Lanz, V. A., Schreiber, D., Mohr, M. and Baltensperger, U.: Identification of the Mass Spectral Signature of Organic Aerosols from Wood Burning Emissions, *Environ. Sci. Technol.*, 41(16), 5770–5777, doi:10.1021/es062289b, 2007.
- Allan, J. D., Delia, A. E., Coe, H., Bower, K. N., Alfarra, M. R. R., Jimenez, J. L., Middlebrook, A. M., Drewnick, F., Onasch, T. B., Canagaratna, M. R., Jayne, J. T. and Worsnop, D. R.: A generalised method for the extraction of chemically resolved mass spectra from Aerodyne aerosol mass spectrometer data, *J. Aerosol Sci.*, 35(7), 909–922, doi:10.1016/j.jaerosci.2004.02.007, 2004.
- Bressi, M., Cavalli, F., Belis, C. A., Putaud, J.-P. P., Fröhlich, R., Martins dos Santos, S., Petralia, E., Prévôt, A. S. H. H., Berico, M., Malaguti, A. and Canonaco, F.: Variations in the chemical composition of the submicron aerosol and in the sources of the organic fraction at a regional background site of the Po Valley (Italy), *Atmos. Chem. Phys.*, 16(20), 12875–12896, doi:10.5194/acp-16-12875-2016, 2016.
- Brown, S. S., Dibb, J. E., Stark, H., Aldener, M., Vozella, M., Whitlow, S., Williams, E. J.,

728 Lerner, B. M., Jakoubek, R., Middlebrook, A. M., DeGouw, J. A., Warneke, C., Goldan, P. D.,  
 729 Kuster, W. C., Angevine, W. M., Sueper, D. T., Quinn, P. K., Bates, T. S., Meagher, J. F.,  
 730 Fehsenfeld, F. C. and Ravishankara, A. R.: Nighttime removal of NO<sub>x</sub> in the summer marine  
 731 boundary layer, *Geophys. Res. Lett.*, 31(7), n/a-n/a, doi:10.1029/2004GL019412, 2004.

732 Canagaratna, M. R., Jayne, J. T., Jimenez, J. L., Allan, J. D., Alfarra, M. R., Zhang, Q., Onasch,  
 733 T. B., Drewnick, F., Coe, H., Middlebrook, A., Delia, A., Williams, L. R., Trimborn, A. M.,  
 734 Northway, M. J., DeCarlo, P. F., Kolb, C. E., Davidovits, P. and Worsnop, D. R.: Chemical  
 735 and microphysical characterisation of ambient aerosols with the aerodyne aerosol mass  
 736 spectrometer, *Mass Spectrom. Rev.*, 26(2), 185–222, doi:10.1002/mas.20115, 2007.

737 Canonaco, F., Crippa, M., Slowik, J. G., Baltensperger, U. and Prévôt, A. S. H. H.: SoFi, an  
 738 IGOR-based interface for the efficient use of the generalised multilinear engine (ME-2) for the  
 739 source apportionment: ME-2 application to aerosol mass spectrometer data, *Atmos. Meas.*  
 740 *Tech.*, 6(12), 3649–3661, doi:10.5194/amt-6-3649-2013, 2013.

741 Canonaco, F., Slowik, J. G., Baltensperger, U. and Prévôt, A. S. H.: Seasonal differences in  
 742 oxygenated organic aerosol composition: implications for emissions sources and factor  
 743 analysis, *Atmos. Chem. Phys.*, 15(12), 6993–7002, doi:10.5194/acp-15-6993-2015, 2015.

744 Canonaco, F., Tobler, A., Chen, G., Sosedova, Y., Slowik, J. G. G., Bozzetti, C., Daellenbach,  
 745 K. R., El Haddad, I., Crippa, M., Huang, R.-J., Furger, M., Baltensperger, U., Prévôt, A. S. H.,  
 746 Kaspar Rudolf Haddad, I. E. D., Crippa, M., Huang, R.-J., Furger, M., Baltensperger, U.,  
 747 Prevot, A. S. H., Daellenbach, Kaspar Rudolf Haddad, I. El, Crippa, M., Huang, R.-J., Furger,  
 748 M., Baltensperger, U. and Prevot, A. S. H.: A new method for long-term source apportionment  
 749 with time-dependent factor profiles and uncertainty assessment using SoFi Pro: application to  
 750 1 year of organic aerosol data, *Atmos. Meas. Tech.*, 14(2), 923–943, doi:10.5194/amt-14-923-  
 751 2021, 2021.



752 Chirico, R., DeCarlo, P. F., Heringa, M. F., Tritscher, T., Richter, R., Prévôt, A. S. H., Dommen,  
 753 J., Weingartner, E., Wehrle, G., Gysel, M., Laborde, M. and Baltensperger, U.: Impact of  
 754 aftertreatment devices on primary emissions and secondary organic aerosol formation potential  
 755 from in-use diesel vehicles: results from smog chamber experiments, *Atmos. Chem. Phys.*,  
 756 10(23), 11545–11563, doi:10.5194/acp-10-11545-2010, 2010.

757 Chow, J. C., Bachmann, J. D., Wierman, S. S. G., Mathai, C. V., Malm, W. C., White, W. H.,  
 758 Mueller, P. K., Kumar, N. and Watson, J. G.: Visibility: Science and Regulation, *J. Air Waste*  
 759 *Manage. Assoc.*, 52(9), 973–999, doi:10.1080/10473289.2002.10470844, 2002.

760 Crippa, M., DeCarlo, P. F., Slowik, J. G., Mohr, C., Heringa, M. F., Chirico, R., Poulain, L.,  
 761 Freutel, F., Sciare, J., Cozic, J., Di Marco, C. F., Elsasser, M., Nicolas, J. B., Marchand, N.,  
 762 Abidi, E., Wiedensohler, A., Drewnick, F., Schneider, J., Borrmann, S., Nemitz, E.,  
 763 Zimmermann, R., Jaffrezo, J.-L., Prévôt, A. S. H. and Baltensperger, U.: Wintertime aerosol  
 764 chemical composition and source apportionment of the organic fraction in the metropolitan  
 765 area of Paris, *Atmos. Chem. Phys.*, 13(2), 961–981, doi:10.5194/acp-13-961-2013, 2013.

766 Crippa, M., Canonaco, F., Lanz, V. A., Äijälä, M., Allan, J. D., Carbone, S., Capes, G.,  
 767 Ceburnis, D., Dall'Osto, M., Day, D. A., DeCarlo, P. F., Ehn, M., Eriksson, A.,  
 768 Freney, E., Hildebrandt Ruiz, L., Hillamo, R., Jimenez, J. L., Junninen, H., Kiendler-Scharr,  
 769 A., Kortelainen, A.-M. M., Kulmala, M., Laaksonen, A., Mensah, A. A., Mohr, C., Nemitz, E.,  
 770 O'Dowd, C., Ovadnevaite, J., Pandis, S. N., Petäjä, T., Poulain, L., Saarikoski, S.,  
 771 Sellegri, K., Swietlicki, E., Tiitta, P., Worsnop, D. R., Baltensperger, U., Prévôt, A. S. H. H.,  
 772 Dall'Osto, M., Day, D. A., DeCarlo, P. F., Ehn, M., Eriksson, A., Freney, E., Hildebrandt Ruiz,  
 773 L., Hillamo, R., Jimenez, J. L., Junninen, H., Kiendler-Scharr, A., Kortelainen, A.-M. M.,  
 774 Kulmala, M., Laaksonen, A., Mensah, A. A., Mohr, C., Nemitz, E., O'Dowd, C., Ovadnevaite,  
 775 J., Pandis, S. N., Petäjä, T., Poulain, L., Saarikoski, S., Sellegri, K., Swietlicki, E., Tiitta, P.,

776 Worsnop, D. R., Baltensperger, U. and Prévôt, A. S. H. H.: Organic aerosol components  
 777 derived from 25 AMS data sets across Europe using a consistent ME-2 based source  
 778 apportionment approach, *Atmos. Chem. Phys.*, 14(12), 6159–6176, doi:10.5194/acp-14-6159-  
 779 2014, 2014.

780 Cubison, M. J. J., Ortega, A. M. M., Hayes, P. L. L., Farmer, D. K. K., Day, D., Lechner, M.  
 781 J. J., Brune, W. H. H., Apel, E., Diskin, G. S., Fisher, J. A., Fuelberg, H. E., Hecobian, A.,  
 782 Knapp, D. J., Mikoviny, T., Riemer, D., Sachse, G. W., Sessions, W., Weber, R. J., Weinheimer,  
 783 A. J., Wisthaler, A. and Jimenez, J. L.: Effects of aging on organic aerosol from open biomass  
 784 burning smoke in aircraft and laboratory studies, *Atmos. Chem. Phys.*, 11(23), 12049–12064,  
 785 doi:www.atmos-chem-phys.net/11/12049/2011/, 2011.

786 Daellenbach, K. R., Bozzetti, C., Křepelová, A., Canonaco, F., Wolf, R., Zotter, P., Fermo, P.,  
 787 Crippa, M., Slowik, J. G., Sosedova, Y., Zhang, Y., Huang, R.-J. J., Poulain, L., Szidat, S.,  
 788 Baltensperger, U., El Haddad, I. and Prévôt, A. S. H. H.: Characterisation and source  
 789 apportionment of organic aerosol using offline aerosol mass spectrometry, *Atmos. Meas. Tech.*,  
 790 9(1), 23–39, doi:10.5194/amt-9-23-2016, 2016.

791 Daellenbach, K. R., Uzu, G., Jiang, J., Cassagnes, L.-E., Leni, Z., Vlachou, A., Stefenelli, G.,  
 792 Canonaco, F., Weber, S., Segers, A., Kuenen, J. J. P., Schaap, M., Favez, O., Albinet, A.,  
 793 Aksoyoglu, S., Dommen, J., Baltensperger, U., Geiser, M., El Haddad, I., Jaffrezo, J.-L. and  
 794 Prévôt, A. S. H.: Sources of particulate-matter air pollution and its oxidative potential in Europe,  
 795 *Nature*, 587(7834), 414–419, doi:10.1038/s41586-020-2902-8, 2020.

796 DeCarlo, P. F., Dunlea, E. J., Kimmel, J. R., Aiken, A. C., Sueper, D., Crounse, J., Wennberg,  
 797 P. O., Emmons, L., Shinozuka, Y., Clarke, A., Zhou, J., Tomlinson, J., Collins, D. R., Knapp,  
 798 D., Weinheimer, A. J., Montzka, D. D., Campos, T. and Jimenez, J. L.: Fast airborne aerosol  
 799 size and chemistry measurements above Mexico City and Central Mexico during the

800 MILAGRO campaign, *Atmos. Chem. Phys.*, 8(14), 4027–4048, doi:10.5194/acp-8-4027-2008,  
801 2008.

802 Dentener, F. J. and Crutzen, P. J.: Reaction of N<sub>2</sub>O<sub>5</sub> on tropospheric aerosols: Impact on the  
803 global distributions of NO<sub>x</sub>, O<sub>3</sub>, and OH, *J. Geophys. Res. Atmos.*, 98(D4), 7149–7163,  
804 doi:10.1029/92JD02979, 1993.

805 Dockery, D. W. and Pope, C. A.: Acute Respiratory Effects of Particulate Air Pollution, *Annu.*  
806 *Rev. Public Health*, 15(1), 107–132, doi:10.1146/annurev.pu.15.050194.000543, 1994.

807 Duplissy, J., DeCarlo, P. F., Dommen, J., Alfarra, M. R., Metzger, A., Barmapadimos, I., Prevot,  
808 A. S. H., Weingartner, E., Tritscher, T., Gysel, M., Aiken, A. C., Jimenez, J. L., Canagaratna,  
809 M. R., Worsnop, D. R., Collins, D. R., Tomlinson, J. and Baltensperger, U.: Relating  
810 hygroscopicity and composition of organic aerosol particulate matter, *Atmos. Chem. Phys.*,  
811 11(3), 1155–1165, doi:10.5194/acp-11-1155-2011, 2011.

812 Efron, B.: Bootstrap Methods: Another Look at the Jackknife, *Ann. Stat.*, 7(1), 1–26 [online]  
813 Available from: <https://www.jstor.org/stable/2958830>, 1979.

814 Fröhlich, R., Cubison, M. J., Slowik, J. G., Bukowiecki, N., Prévôt, A. S. H. H., Baltensperger,  
815 U., Schneider, J., Kimmel, J. R., Gonin, M., Rohner, U., Worsnop, D. R. and Jayne, J. T.: The  
816 ToF-ACSM: a portable aerosol chemical speciation monitor with TOFMS detection, *Atmos.*  
817 *Meas. Tech.*, 6(11), 3225–3241, doi:10.5194/amt-6-3225-2013, 2013.

818 Fröhlich, R., Crenn, V., Setyan, A., Belis, C. A., Canonaco, F., Favez, O., Riffault, V., Slowik,  
819 J. G., Aas, W., Aijälä, M., Alastuey, A., Artiñano, B., Bonnaire, N., Bozzetti, C., Bressi, M.,  
820 Carbone, C., Coz, E., Croteau, P. L., Cubison, M. J., Esser-Gietl, J. K., Green, D. C., Gros, V.,  
821 Heikkinen, L., Herrmann, H., Jayne, J. T., Lunder, C. R., Minguillón, M. C., Močnik, G.,  
822 O'Dowd, C. D., Ovadnevaite, J., Petralia, E., Poulain, L., Priestman, M., Ripoll, A., Sarda-

823 Estève, R., Wiedensohler, A., Baltensperger, U., Sciare, J., Prévôt, A. S. H.,  
824 O&apos;Dowd, C. D., Ovadnevaite, J., Petralia, E., Poulain, L., Priestman, M., Ripoll, A.,  
825 Sarda-Estève, R., Wiedensohler, A., Baltensperger, U., Sciare, J., Prévôt, A. S. H., O’Dowd,  
826 C. D., Ovadnevaite, J., Petralia, E., Poulain, L., Priestman, M., Ripoll, A., Sarda-Estève, R.,  
827 Wiedensohler, A., Baltensperger, U., Sciare, J. and Prévôt, A. S. H.: ACTRIS ACSM  
828 intercomparison – Part 2: Intercomparison of ME-2 organic source apportionment results from  
829 15 individual, co-located aerosol mass spectrometers, *Atmos. Meas. Tech.*, 8(6), 2555–2576,  
830 doi:10.5194/amt-8-2555-2015, 2015.

831 Heringa, M. F., DeCarlo, P. F., Chirico, R., Tritscher, T., Dommen, J., Weingartner, E., Richter,  
832 R., Wehrle, G., Prévôt, A. S. H. and Baltensperger, U.: Investigations of primary and secondary  
833 particulate matter of different wood combustion appliances with a high-resolution time-of-  
834 flight aerosol mass spectrometer, *Atmos. Chem. Phys.*, 11(12), 5945–5957, doi:10.5194/acp-  
835 11-5945-2011, 2011.

836 Hildebrandt, L., Kostenidou, E., Lanz, V. A., Prevot, A. S. H. H., Baltensperger, U.,  
837 Mihalopoulos, N., Laaksonen, A., Donahue, N. M. and Pandis, S. N.: Sources and atmospheric  
838 processing of organic aerosol in the Mediterranean: insights from aerosol mass spectrometer  
839 factor analysis, *Atmos. Chem. Phys.*, 11(23), 12499–12515, doi:10.5194/acp-11-12499-2011,  
840 2011.

841 Horvath, H.: Atmospheric light absorption—A review, *Atmos. Environ. Part A. Gen. Top.*,  
842 27(3), 293–317, doi:10.1016/0960-1686(93)90104-7, 1993.

843 Hüglin, C. and Grange, S. K.: Chemical characterisation and source identification, Dübendorf,  
844 Zurich. [online] Available from:  
845 <https://www.aramis.admin.ch/Default?DocumentID=67473&Load=true>, 2021.

846 IPCC: Clouds and Aerosols, in *Climate Change 2013 - The Physical Science Basis*, edited by  
 847 Intergovernmental Panel on Climate Change, pp. 571–658, Cambridge University Press,  
 848 Cambridge., 2014.

849 Jacobson, M. C., Hansson, H.-C., Noone, K. J. and Charlson, R. J.: Organic atmospheric  
 850 aerosols: Review and state of the science, *Rev. Geophys.*, 38(2), 267–294,  
 851 doi:10.1029/1998RG000045, 2000.

852 Jacobson, M. Z.: Global direct radiative forcing due to multicomponent anthropogenic and  
 853 natural aerosols, *J. Geophys. Res. Atmos.*, 106(D2), 1551–1568, doi:10.1029/2000JD900514,  
 854 2001.

855 Jimenez, J. L., Canagaratna, M. R., Donahue, N. M., Prevot, A. S. H. H., Zhang, Q., Kroll, J.  
 856 H., DeCarlo, P. F., Allan, J. D., Coe, H., Ng, N. L., Aiken, A. C., Docherty, K. S., Ulbrich, I.  
 857 M., Grieshop, A. P., Robinson, A. L., Duplissy, J., Smith, J. D., Wilson, K. R., Lanz, V. A.,  
 858 Hueglin, C., Sun, Y. L., Tian, J., Laaksonen, A., Raatikainen, T., Rautiainen, J., Vaattovaara,  
 859 P., Ehn, M., Kulmala, M., Tomlinson, J. M., Collins, D. R., Cubison, M. J., Dunlea, E. J.,  
 860 Huffman, J. A., Onasch, T. B., Alfarra, M. R., Williams, P. I., Bower, K., Kondo, Y., Schneider,  
 861 J., Drewnick, F., Borrmann, S., Weimer, S., Demerjian, K., Salcedo, D., Cottrell, L., Griffin,  
 862 R., Takami, A., Miyoshi, T., Hatakeyama, S., Shimono, A., Sun, J. Y., Zhang, Y. M., Dzepina,  
 863 K., Kimmel, J. R., Sueper, D., Jayne, J. T., Herndon, S. C., Trimborn, A. M., Williams, L. R.,  
 864 Wood, E. C., Middlebrook, A. M., Kolb, C. E., Baltensperger, U., Worsnop, D. R., Dunlea, J.,  
 865 Huffman, J. A., Onasch, T. B., Alfarra, M. R., Williams, P. I., Bower, K., Kondo, Y., Schneider,  
 866 J., Drewnick, F., Borrmann, S., Weimer, S., Demerjian, K., Salcedo, D., Cottrell, L., Griffin,  
 867 R., Takami, A., Miyoshi, T., Hatakeyama, S., Shimono, A., Sun, J. Y., Zhang, Y. M., Dzepina,  
 868 K., Kimmel, J. R., Sueper, D., Jayne, J. T., Herndon, S. C., Trimborn, A. M., Williams, L. R.,  
 869 Wood, E. C., Middlebrook, A. M., Kolb, C. E., Baltensperger, U., Worsnop, D. R., Dunlea, E.

870 J., Huffman, J. A., et al.: Evolution of organic aerosols in the atmosphere, *Science* (80-. ),  
871 326(5959), 1525–1529, doi:10.1126/science.1180353, 2009.

872 Lanz, V. A., Alfarra, M. R., Baltensperger, U., Buchmann, B., Hueglin, C. and Prévôt, A. S.  
873 H.: Source apportionment of submicron organic aerosols at an urban site by factor analytical  
874 modelling of aerosol mass spectra, *Atmos. Chem. Phys.*, 7(6), 1503–1522, doi:10.5194/acp-7-  
875 1503-2007, 2007.

876 Lanz, V. A., Alfarra, M. R., Baltensperger, U., Buchmann, B., Hueglin, C., Szidat, S., Wehrli,  
877 M. N., Wacker, L., Weimer, S., Caseiro, A., Puxbaum, H. and Prevot, A. S. H.: Source  
878 Attribution of Submicron Organic Aerosols during Wintertime Inversions by Advanced Factor  
879 Analysis of Aerosol Mass Spectra, *Environ. Sci. Technol.*, 42(1), 214–220,  
880 doi:10.1021/es0707207, 2008.

881 Lelieveld, J., Evans, J. S., Fnais, M., Giannadaki, D. and Pozzer, A.: The contribution of  
882 outdoor air pollution sources to premature mortality on a global scale, *Nature*, 525(7569), 367–  
883 371, doi:10.1038/nature15371, 2015.

884 Matthew, B. M., Middlebrook, A. M. and Onasch, T. B.: Collection Efficiencies in an  
885 Aerodyne Aerosol Mass Spectrometer as a Function of Particle Phase for Laboratory Generated  
886 Aerosols, *Aerosol Sci. Technol.*, 42(11), 884–898, doi:10.1080/02786820802356797, 2008.

887 Mauderly, J. L. and Chow, J. C.: Health Effects of Organic Aerosols, *Inhal. Toxicol.*, 20(3),  
888 257–288, doi:10.1080/08958370701866008, 2008.

889 Meteotest: Data Report Switzerland 2007 – 2016, Bern, Switzerland., 2017.

890 Minguillón, M. C., Ripoll, A., Pérez, N., Prévôt, A. S. H. H., Canonaco, F., Querol, X. and  
891 Alastuey, A.: Chemical characterisation of submicron regional background aerosols in the  
892 western Mediterranean using an Aerosol Chemical Speciation Monitor, *Atmos. Chem. Phys.*,

893 15(11), 6379–6391, doi:10.5194/acp-15-6379-2015, 2015.

894 Mohr, C., Decarlo, P. F., Heringa, M. F., Chirico, R., Slowik, J. G., Richter, R., Reche, C.,  
895 Alastuey, A., Querol, X., Seco, R., Crippa, M., Zimmermann, R., Baltensperger, U., Barcelona,  
896 D., Munchen, H. Z. and Mass, J.: Wintertime aerosol chemical composition and source  
897 apportionment of the organic fraction in the metropolitan area of Paris, *Atmos. Chem. Phys.*,  
898 12(4), 1649–1665, doi:10.5194/acp-13-961-2013, 2012.

899 Monn, C.: Exposure assessment of air pollutants: a review on spatial heterogeneity and  
900 indoor/outdoor/personal exposure to suspended particulate matter, nitrogen dioxide and ozone,  
901 *Atmos. Environ.*, 35(1), 1–32, doi:10.1016/S1352-2310(00)00330-7, 2001.

902 Murphy, D. M., Cziczo, D. J., Froyd, K. D., Hudson, P. K., Matthew, B. M., Middlebrook, A.  
903 M., Peltier, R. E., Sullivan, A., Thomson, D. S. and Weber, R. J.: Single-particle mass  
904 spectrometry of tropospheric aerosol particles, *J. Geophys. Res. Atmos.*, 111(D23), n/a-n/a,  
905 doi:10.1029/2006JD007340, 2006.

906 Ng, N. L., Canagaratna, M. R., Zhang, Q., Jimenez, J. L., Tian, J., Ulbrich, I. M., Kroll, J. H.,  
907 Docherty, K. S., Chhabra, P. S., Bahreini, R., Murphy, S. M., Seinfeld, J. H., Hildebrandt, L.,  
908 Donahue, N. M., DeCarlo, P. F., Lanz, V. A., Prévôt, A. S. H. H., Dinar, E., Rudich, Y. and  
909 Worsnop, D. R.: Organic aerosol components observed in Northern Hemispheric datasets from  
910 Aerosol Mass Spectrometry, *Atmos. Chem. Phys.*, 10(10), 4625–4641, doi:10.5194/acp-10-  
911 4625-2010, 2010.

912 Ng, N. L., Herndon, S. C., Trimborn, A., Canagaratna, M. R., Croteau, P. L., Onasch, T. B.,  
913 Sueper, D., Worsnop, D. R., Zhang, Q., Sun, Y. L. and Jayne, J. T.: An Aerosol Chemical  
914 Speciation Monitor (ACSM) for Routine Monitoring of the Composition and Mass  
915 Concentrations of Ambient Aerosol, *Aerosol Sci. Technol.*, 45(7), 780–794,

doi:10.1080/02786826.2011.560211, 2011a.

Ng, N. L., Canagaratna, M. R., Jimenez, J. L., Zhang, Q., Ulbrich, I. M. and Worsnop, D. R.: Real-Time Methods for Estimating Organic Component Mass Concentrations from Aerosol Mass Spectrometer Data, *Environ. Sci. Technol.*, 45(3), 910–916, doi:10.1021/es102951k, 2011b.

NIST Mass Spectrometry Data Center: Disulfide, dimethyl, SRD 69. [online] Available from: <https://webbook.nist.gov/cgi/cbook.cgi?ID=C624920&Mask=200#Refs> (Accessed 6 August 2020), 2014.

Paatero, P.: The Multilinear Engine—A Table-Driven, Least Squares Program for Solving Multilinear Problems, Including the n -Way Parallel Factor Analysis Model, *J. Comput. Graph. Stat.*, 8(4), 854–888, doi:10.1080/10618600.1999.10474853, 1999.

Paatero, P. and Hopke, P. K.: Discarding or downweighting high-noise variables in factor analytic models, *Anal. Chim. Acta*, 490(1–2), 277–289, doi:10.1016/S0003-2670(02)01643-4, 2003.

Paatero, P., Eberly, S., Brown, S. G. and Norris, G. A.: Methods for estimating uncertainty in factor analytic solutions, *Atmos. Meas. Tech.*, 7(3), 781–797, doi:10.5194/amt-7-781-2014, 2014.

Parworth, C., Fast, J., Mei, F., Shippert, T., Sivaraman, C., Tilp, A., Watson, T. and Zhang, Q.: Long-term measurements of submicrometer aerosol chemistry at the Southern Great Plains (SGP) using an Aerosol Chemical Speciation Monitor (ACSM), *Atmos. Environ.*, 106, 43–55, doi:10.1016/j.atmosenv.2015.01.060, 2015.

Petit, J.-E. E., Favez, O., Sciare, J., Canonaco, F., Croteau, P., Močnik, G., Jayne, J., Worsnop, D. and Leoz-Garziandia, E.: Submicron aerosol source apportionment of wintertime pollution



939 in Paris, France by double positive matrix factorisation (PMF2) using an aerosol chemical  
 940 speciation monitor (ACSM) and a multi-wavelength Aethalometer, *Atmos. Chem. Phys.*,  
 941 14(24), 13773–13787, doi:10.5194/acp-14-13773-2014, 2014.

942 Pfaffenberger, L., Barmet, P., Slowik, J. G., Praplan, A. P., Dommen, J., Prévôt, A. S. H. and  
 943 Baltensperger, U.: The link between organic aerosol mass loading and degree of oxygenation:  
 944 an  $\alpha$ -pinene photooxidation study, *Atmos. Chem. Phys.*, 13(13), 6493–6506, doi:10.5194/acp-  
 945 13-6493-2013, 2013.

946 Pope, C. A. and Dockery, D. W.: Health Effects of Fine Particulate Air Pollution: Lines that  
 947 Connect, J. Air Waste Manage. Assoc., 56(6), 709–742,  
 948 doi:10.1080/10473289.2006.10464485, 2006.

949 Ramanathan, V., Chung, C., Kim, D., Bettge, T., Buja, L., Kiehl, J. T., Washington, W. M., Fu,  
 950 Q., Sikka, D. R. and Wild, M.: Atmospheric brown clouds: Impacts on South Asian climate  
 951 and hydrological cycle, *Proc. Natl. Acad. Sci.*, 102(15), 5326–5333,  
 952 doi:10.1073/pnas.0500656102, 2005.

953 Reyes-Villegas, E., Green, D. C., Priestman, M., Canonaco, F., Coe, H., Prévôt, A. S. H. H.  
 954 and Allan, J. D.: Organic aerosol source apportionment in London 2013 with ME-2: Exploring  
 955 the solution space with annual and seasonal analysis, *Atmos. Chem. Phys.*, 16(24), 15545–  
 956 15559, doi:10.5194/acp-16-15545-2016, 2016.

957 Ripoll, A., Minguillón, M. C., Pey, J., Jimenez, J. L., Day, D. A., Sosedova, Y., Canonaco, F.,  
 958 Prévôt, A. S. H., Querol, X. and Alastuey, A.: Long-term real-time chemical characterisation  
 959 of submicron aerosols at Montsec (southern Pyrenees, 1570 m a.s.l.), *Atmos. Chem. Phys.*,  
 960 15(6), 2935–2951, doi:10.5194/acp-15-2935-2015, 2015.

961 von Schneidmesser, E., Monks, P. S., Allan, J. D., Bruhwiler, L., Forster, P., Fowler, D., Lauer,

962 A., Morgan, W. T., Paasonen, P., Righi, M., Sindelarova, K. and Sutton, M. A.: Chemistry and  
 963 the Linkages between Air Quality and Climate Change, *Chem. Rev.*, 115(10), 3856–3897,  
 964 doi:10.1021/acs.chemrev.5b00089, 2015.

965 Schurman, M. I., Lee, T., Sun, Y., Schichtel, B. A., Kreidenweis, S. M. and Collett Jr., J. L.:  
 966 Investigating types and sources of organic aerosol in Rocky Mountain National Park using  
 967 aerosol mass spectrometry, *Atmos. Chem. Phys.*, 15(2), 737–752, doi:10.5194/acp-15-737-  
 968 2015, 2015.

969 Schwarz, J. P., Gao, R. S., Perring, A. E., Spackman, J. R. and Fahey, D. W.: Black carbon  
 970 aerosol size in snow, *Sci. Rep.*, 3, 1–5, doi:10.1038/srep01356, 2013.

971 Sug Park, E., Henry, R. C. and Spiegelman, C. H.: Estimating the number of factors to include  
 972 in a high-dimensional multivariate bilinear model, *Commun. Stat. - Simul. Comput.*, 29(3),  
 973 723–746, doi:10.1080/03610910008813637, 2000.

974 Szidat, S., Prévôt, A. S. H., Sandradewi, J., Alfarra, M. R., Synal, H.-A., Wacker, L. and  
 975 Baltensperger, U.: Dominant impact of residential wood burning on particulate matter in  
 976 Alpine valleys during winter, *Geophys. Res. Lett.*, 34(5), doi:10.1029/2006GL028325, 2007.

977 The Swiss Federal Council: Ordinance of 16 December 1985 on Air Pollution Control (OAPC).  
 978 [online] Available from: [https://www.admin.ch/opc/en/classified-](https://www.admin.ch/opc/en/classified-compilation/19850321/index.html#app7)  
 979 [compilation/19850321/index.html#app7](https://www.admin.ch/opc/en/classified-compilation/19850321/index.html#app7) (Accessed 10 September 2019), 2018.

980 Tobler, A., Bhattu, D., Canonaco, F., Lalchandani, V., Shukla, A., Thamban, N. M., Mishra,  
 981 S., Srivastava, A. K., Bisht, D. S., Tiwari, S., Singh, S., Močnik, G., Baltensperger, U., Tripathi,  
 982 S. N., Slowik, J. G. and Prévôt, A. S. H.: Chemical characterisation of PM<sub>2.5</sub> and source  
 983 apportionment of organic aerosol in New Delhi, India, *Sci. Total Environ.*, 745, 140924,  
 984 doi:10.1016/j.scitotenv.2020.140924, 2020.

985 Ulbrich, I. M., Canagaratna, M. R., Zhang, Q., Worsnop, D. R. and Jimenez, J. L.:  
 986 Interpretation of organic components from Positive Matrix Factorization of aerosol mass  
 987 spectrometric data, *Atmos. Chem. Phys.*, 9(9), 2891–2918, doi:10.5194/acp-9-2891-2009,  
 988 2009.

989 Via, M., Chen, G. and Minguillón, M. C.: Comparison between rolling and seasonal PMF  
 990 techniques for organic aerosol source apportionment., 2021.

991 Vlachou, A., Daellenbach, K. R., Bozzetti, C., Chazeau, B., Salazar, G. A., Szidat, S., Jaffrezo,  
 992 J.-L., Hueglin, C., Baltensperger, U., Haddad, I. El and Prévôt, A. S. H.: Advanced source  
 993 apportionment of carbonaceous aerosols by coupling offline AMS and radiocarbon size-  
 994 segregated measurements over a nearly 2-year period, *Atmos. Chem. Phys.*, 18(9), 6187–6206,  
 995 doi:10.5194/acp-18-6187-2018, 2018.

996 Zhang, Q., Jimenez, J. L., Canagaratna, M. R., Allan, J. D., Coe, H., Ulbrich, I., Alfarra, M. R.,  
 997 Takami, A., Middlebrook, A. M., Sun, Y. L., Dzepina, K., Dunlea, E., Docherty, K., DeCarlo,  
 998 P. F., Salcedo, D., Onasch, T., Jayne, J. T., Miyoshi, T., Shimojo, A., Hatakeyama, S.,  
 999 Takegawa, N., Kondo, Y., Schneider, J., Drewnick, F., Borrmann, S., Weimer, S., Demerjian,  
 1000 K., Williams, P., Bower, K., Bahreini, R., Cottrell, L., Griffin, R. J., Rautiainen, J., Sun, J. Y.,  
 1001 Zhang, Y. M. and Worsnop, D. R.: Ubiquity and dominance of oxygenated species in organic  
 1002 aerosols in anthropogenically-influenced Northern Hemisphere midlatitudes, *Geophys. Res.*  
 1003 *Lett.*, 34(13), n/a-n/a, doi:10.1029/2007GL029979, 2007.

1004 Zhang, Q., Jimenez, J. L., Canagaratna, M. R., Ulbrich, I. M., Ng, N. L., Worsnop, D. R. and  
 1005 Sun, Y.: Understanding atmospheric organic aerosols via factor analysis of aerosol mass  
 1006 spectrometry: a review, *Anal. Bioanal. Chem.*, 401(10), 3045–3067, doi:10.1007/s00216-011-  
 1007 5355-y, 2011.

1008 Zhang, Y., Favez, O., Petit, J.-E., Canonaco, F., Truong, F., Bonnaire, N., Crenn, V., Amodeo,  
 1009 T., Prévôt, A. S. H., Sciare, J., Gros, V. and Albinet, A.: Six-year source apportionment of  
 1010 submicron organic aerosols from near-continuous highly time-resolved measurements at  
 1011 SIRTa (Paris area, France), *Atmos. Chem. Phys.*, 19(23), 14755–14776, doi:10.5194/acp-19-  
 1012 14755-2019, 2019.

1013 Zotter, P., Herich, H., Gysel, M., El-Haddad, I., Zhang, Y., Močnik, G., Hüglin, C.,  
 1014 Baltensperger, U., Szidat, S., Prévôt, A. S. H. H., Mocnik, G., Hüglin, C., Baltensperger, U.,  
 1015 Szidat, S., Prévôt, A. S. H. H., Močnik, G., Hüglin, C., Baltensperger, U., Szidat, S. and Prévôt,  
 1016 A. S. H. H.: Evaluation of the absorption Ångström exponents for traffic and wood burning in  
 1017 the Aethalometer-based source apportionment using radiocarbon measurements of ambient  
 1018 aerosol, *Atmos. Chem. Phys.*, 17(6), 4229–4249, doi:10.5194/acp-17-4229-2017, 2017.

1019